ABSTRACT

Title of Thesis: **CONTROL OF SIZE AND MAGNETIC PROPERTIES OF CARBOXYL-FUNCTIONALIZED MAGNETITE PARTICLES: SYNTHESIS PROCEDURES, CHARACTERIZATIONS, AND APPLICATIONS**

Yingying Song, Master of Science, 2016

Thesis Directed By: Associate Professor Qin Wang
Department of Nutrition and Food Science

Magnetic nanoparticles (MNPs) are known for the unique properties conferred by their small size and have found wide application in food safety analyses. However, their high surface energy and strong magnetization often lead to aggregation, compromising their functions. In this study, iron oxide magnetic particles (MPs) over the range of nano to micro size were synthesized, from which particles with less aggregation and excellent magnetic properties were obtained. MPs were synthesized via three different hydrothermal procedures, using poly (acrylic acid) (PAA) of different molecular weight (Mw) as the stabilizer. The particle size, morphology, and magnetic properties of the MPs from these synthesis procedures were characterized and compared. Among the three syntheses, one-step hydrothermal synthesis demonstrated the highest yield and most efficient magnetic collection of the resulting PAA-coated magnetic microparticles (PAA-MMPs, >100 nm). Iron oxide content of these PAA-MMPs was around 90%, and the saturation magnetization ranged from

70.3 emu/g to 57.0 emu/g, depending on the Mw of PAA used. In this approach, the particles prepared using PAA with Mw of 100K g/mol exhibited super-paramagnetic behavior with ~65% lower coercivity and remanence compared to others. They were therefore less susceptible to aggregation and remained remarkably water-dispersible even after one-month storage. Three applications involving PAA-MMPs from one-step hydrothermal synthesis were explored: food proteins and enzymes immobilization, antibody conjugation for pathogen capture, and magnetic hydrogel film fabrication. These studies demonstrated their versatile functions as well as their potential applications in the food science area.

CONTROL OF SIZE AND MAGNETIC PROPERTIES OF CARBOXYL-FUNCTIONALIZED MAGNETITE PARTICLES: SYNTHESIS PROCEDURES, CHARACTERIZATIONS, AND APPLICATIONS

by

Yingying Song

Thesis submitted to the Faculty of the Graduate School of the
University of Maryland, College Park, in partial fulfillment
of the requirements for the degree of
Master of Science
2016

Advisory Committee:
Dr. Qin Wang, Chair
Dr. Thomas W. Castonguay
Dr. Rohan V. Tikekar

Acknowledgements

I would like to express my sincerest gratitude to certain individuals who provide kind and constant assistance during my master studies and the completion of this thesis. It would not be possible to finish my master thesis without the guidance and support from these people.

First of all, I would like to express my greatest gratitude to my advisor, Dr. Qin Wang, for this opportunity to study in her group. Dr. Wang continually shared her expertise with me, guided me through my graduate studies both in research and courses, and provided me with wonderful research projects that really enriched my interdisciplinary knowledge and broadened my horizon. It was my great honor to be part of her lab. My appreciation also goes to Dr. Thomas W. Castonguay and Dr. Rohan V. Tikekar for serving on my Graduate Advisory Committee. I appreciate their generous support and vital inspirations.

I would also like to express my deep thanks to Dr. Ying Li, Dr. Zi Teng, and Dr. Yi Liu, who always supported me with their best capability and endless assistance. I have learned a lot from their expertise as well as working attitudes. It was my pleasure to have them by my side. I acknowledge Dr. Sz Chian Liou, Dr. Tieren Gao, and Dr. Isabel K. Lloyd for their expert advices and generous assistance with their lab equipment. I also give special thanks to Sara Kao, Marythai Pandian, other faculty and staff that I worked with for their kindly help and encouragement during my studies at the University of Maryland. Without all these people, I would not be studying and working here enjoyably and fruitfully. I also want to express my

appreciation to my fellowship brothers and sisters, who provided faithful support and encouragement, and who showed love and care all the time.

Most importantly, I owe my deepest thanks to my family for their unconditional love, greatest understanding, and immense support during prosperity as well as adversity. They not only educated me like experienced tutors, but also share their stories and showed care for me like friends. They have not said a word about my being in another country thus temporary unable to take care of them. It is beyond my words that how lucky I feel and how grateful I am for being part of this family.

Last but not least, I appreciate the University of Maryland and the Department of Nutrition and Food Science for the great academic environment as well as the generous financial support being offered. The study and work experiences I acquired here equipped me with the imperative traits that will benefit my entire life.

Table of Contents

List of Tables

List of Figures

Chapter 1: Introduction

1.1 Overview of Magnetic Nanoparticles

Nanoparticles usually have a size between 1-100 nm by definition, extending to several hundred nanometers sometimes. Magnetic materials are those that can be magnetized and can respond to an external magnetic field. The most well-known are iron, nickel, and cobalt, etc. Magnetic materials are classified into five categories based on their magnetic properties, namely, ferromagnetic, paramagnetic, diamagnetic, antiferromagnetic, and ferrimagnetic [1]. Of the five, ferromagnetic and paramagnetic materials have been the most researched. A ferromagnetic material often consists of multiple domains (size of each > 100 nm), exhibiting net zero magnetic moment due to the randomly distributed magnetic moments in domains [1]. An external magnetic field can align all of its magnetic moments along a certain direction and thus induce its magnetism, which will last even when the magnetic field is removed. A permanent magnet made of iron is an example of ferromagnetic material. A paramagnetic magnetic material does not have multiple magnetic domains and demonstrates weak magnetism when an external magnetic field is applied. In contrast to ferromagnetic materials, the aligned magnetic moments disappear after the magnetic field is removed, and show no magnetism [1]. Diamagnetic materials contain zero net magnetic moment, but can display a weak repulsion against the applied magnetic field [1]. The behavior of antiferromagnetic and ferrimagnetic materials are similar to that of ferromagnetic materials [1]. Synthesis of particles with exceptional

magnetic properties is vital to applications that strongly require easy manipulation of the MPs.

Magnetic nanoparticles (MNPs) have been investigated widely in the past decades because of their unique size-dependent physical, chemical, and mechanical properties. The nature for the novel properties of MNPs lies in their high surface-to-volume ratio when particle size decreases to nanoscale, which leads to increased percentage of constituting atoms residing on the surface of nanocrystals [1, 2]. Below a critical size, the domain walls that exist in the bulk ferrite materials are not able to be formed any more, limited by the demanded energy [1]. Instead, single domain particles can be generated, further resulting in super-paramagnetism [3], spin canting [4, 5], and extra magnetic anisotropy [6], which are dissimilar with their correspondent bulk material. When the size decreases to below a critical value, MNPs could be composed of a single domain. When above the blocking temperature, which is material and size specific, the thermal fluctuation is sufficient to overcome the anisotropy energy and disturb the orientation of magnetic moments of MNPs. In this case, MNPs demonstrate super-paramagnetic behavior with high susceptibility and saturation magnetization when an external magnetic field is present, and without remanence magnetization and coercivity when the magnetic field is removed [1]. This behavior confers MNPs with extraordinary magnetic properties, but lessens their aggregation due to dipole-dipole magnetic interaction among individual particles.

The PAA-coated iron oxide (Fe_3O_4) MPs discussed in this thesis will be referred to as PAA-MNPs (< 100 nm) and PAA-MMPs (> 100 nm), respectively.

1.2 Synthesis of Magnetic Nanoparticles

Iron oxide MPs have been synthesized via many synthesis methods in the past, mainly comprising co-precipitation, microemulsion, thermal decomposition, and hydrothermal synthesis [7, 8]. Co-precipitation has been used the most widely, which generates Fe_3O_4 crystals by simply mixing ferric and ferrous ions (molar ratio=1:2) in a high pH solution under room temperature or slightly above (usually < 100°C). Although the condition of this synthesis is the mildest, the size and morphology of the yielded particles are easily affected by various experimental parameters, including the involved salt type, molar ratio of ferric and ferrous ions, reaction pH, synthesis temperature, and the adding rate of base into reaction solution, etc. Moreover, the produced Fe_3O_4 MNPs are highly prone to oxidation into γ-Fe_2O_3 if oxygen is not eliminated during the synthesis process. It is challenging to control and balance all these factors, and the resulted particles usually span a wide range of size with compromised magnetic properties [8]. Microemulsion takes advantage of an isotropic and thermo-dynamically steady single-phase system that involves a water phase, an oil phase, and surfactants [9]. This synthesis follows a similar nucleation process as co-precipitation aforementioned; hence, the same concerns as well as a complicated procedure exist [9]. The size of the created emulsion nanodroplets, within which the MNPs are produced, needs to be strictly regulated, as it greatly affects the size of the resulting MNPs [10].

Thermal decomposition and hydrothermal synthesis are often used to produce monodisperse Fe_3O_4 MNPs. Thermal decomposition involves pyrolysis of an iron precursor in an organic solvent (mostly above 250°C) [11-13]. Thermal decomposition

has achieved the controllable synthesis of monodisperse Fe_3O_4 MNPs less than 10 nm with narrow size distribution [14, 15]. Disadvantages of this synthesis are the tedious synthesis procedures as well as the fastidious ion precursors, which sometimes are highly toxic [12]. Also, the yielded particles are not able to dissolve well in polar solvents, which prohibits a lot of potential functions or requires further surface modification [8].

Compared to the other synthesis approaches, the hydrothermal approach is relatively facile and effective, requiring only simple ingredients, equipment, and synthesis procedures. It is usually performed at high temperature (about 130 to 250°C) and high vapor pressure (about 0.3 to 4 MPa), yielding MNPs with better crystallinity and morphology, higher phase homogeneity [16], and narrower size distribution [8]. As a consequence, hydrothermal synthesis was adopted in this study.

1.3 Surface Modification of Magnetic Nanoparticles

Despite the promising features that MNPs offer, their high surface energy and strong magnetization can easily result in aggregation through hydrophobic interaction, *van der Waals* attraction, and magnetic interaction of individual particles [7, 8]. These forces may lead to unfavorable particle size increase of MNPs, thus compromising their physiochemical properties and other attributes [8, 17, 18]. Although some MNPs such as Fe_3O_4 are non-toxic, there may be issues with immune clearance and cytotoxicity, especially when developing biomedical applications. Therefore, studies have been frequently conducted on the surface modification of the MNPs in order to circumvent direct contact between individual MNPs as well as to decrease the exposure of bare MNPs' surfaces. Surface modification is often achieved by

constructing physical barriers and introducing electrostatically charged functional groups on MNPs, which reduce their high surface energy and counteract their interactions.

The most considerable efforts have been devoted to developing MNPs with charged surface functional groups, which could lower the likelihood of direct collision among MNPs and thus decrease aggregation by electrostatic repulsion among particles. Several charged groups that have been built on MNPs include hydroxyl groups, amine groups, carboxyl groups, aldehyde groups, and thiol groups [18-21], etc. In addition to conferring the MNPs with higher stability, these introduced functional groups may also enhance the surface reactivity of the MNPs, such as their capability of conjugating with various proteins, antibodies, and DNA molecules through chemical cross-linkers. Thus, the applications of these modified MNPs are expanded compared to the unmodified particles because of their stability as well as the ease with which they can be associated with various biomolecules. Moreover, surface modification of MNPs also increases their biocompatibility. For instance, bare MNPs applied in drug delivery may be quickly cleared from the circulation by the mononuclear phagocyte system, or rapidly aggregate into a vast size [22]. Therefore, functionalized and stabilized MNPs could more easily escape the clearing mechanism and assist transporting drugs or nutraceuticals to the targeted cells or organs. It was found that MNPs coated by polyethylene glycol (PEG) achieved outstanding biocompatibility, with extended blood circulation time, reduced immunogenicity, and reduced antigenicity [23, 24]. Some other surface modification using biological molecules such as proteins [8, 25] and polypeptides [26] can also notably improve the

biocompatibility and reduce the cytotoxicity of MNPs. Last but not least, the functionalized MNPs may possess improved water dispersibility, which eases their applications in water-based systems [17].

Both organic and inorganic components have been employed as the coating agents or stabilizers for MNPs in surface modification. Small molecules, polymers, and above-mentioned biological molecules are three regularly researched categories of organic materials. Modification using hydrophilic as well as hydrophobic small molecules is the most widely adopted. The amphiphilic oleic acid with a kink located in the middle of the molecule was demonstrated to successfully stabilize uniform and monodisperse ferrite particles [27, 28]. A lot of hydrophilic substances like citric acid [29] and amino acids [30] are also conjugated on MNPs to improve the hydrophilicity and biocompatibility of MNPs. Small molecules do not significantly increase the size of MNPs or affect their saturation magnetization (M_s) [8]. However, these molecules are susceptible to harsh synthesis or storage environment. Using polymers as stabilizers can provide greater repulsive forces between particles and overcome some of the aforementioned weaknesses of small molecules, especially the synthetic polymers, which can withstand fastidious synthesis conditions. However, the magnetic properties of resulting MNPs may be weakened by non-magnetic macromolecules. Some examples of polymers studied include dextran [24], chitosan [31], PEG [23, 24], and PAA [32, 33], etc.

The typical structures of MNPs modified by organic materials were proposed previously, mainly comprising core-shell, matrix, and $shell_a$-core-$shell_b$ (Figure 1.1) [8]. Coating organic materials onto the present MNPs often creates core-shell structures.

Similarly, mosaic structure consists of MNPs cores embedded in an organic shell, which is commonly a polymer matrix. By contrast, in shell-core structure, MNPs as the shell are chemically bound to an organic core. Coating the shell-core structure with another organic layer using the same or a different component further generates the $shell_a$-core-$shell_b$ structure.

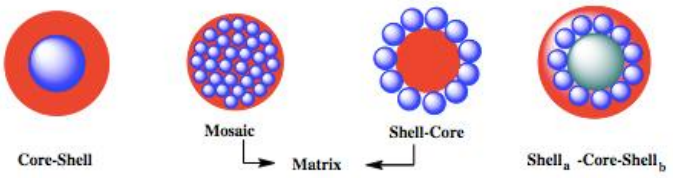

Figure 1.1 Typical structures of MNPs (blue) modified by organic materials (red)

[Used from Ref 8 with permission of Springer]

MNPs involving inorganic stabilizing materials are generally less biocompatible. However, functionalized MNPs are more resistant to oxidation and offer innovative functions. The most commonly engaged inorganic materials include silica, metal, nonmetal, metal oxides, and sulfides [8]. Silica coated MNPs have been well investigated. One of their advantages is that the thickness of silica coating can be easily controlled [8]. Metals are another common type of inorganic coating agent. For instance, gold exhibits excellent anti-oxidation of coated MNPs as well as strong affinity for biomolecules containing thiol groups [34]. Metal coated MNPs are also involved in many other catalytic, bio-separation, and bio-labeling purposes [8, 35]. MNPs coated with metal oxides are often imparted with novel properties such as optical and electrical functions [36]. The typical structures of MNPs modified by inorganic materials were reported previously, including core-shell, mosaic, shell-core,

shell- core-shell, and dumbbell (Figure 1.2) [8]. A hollow mosaic structure is commonly found when MNPs are synthesized in hollow silica spheres. Dumbbells are formed via epitaxial growth of MNPs on inorganic particles or vice versa.

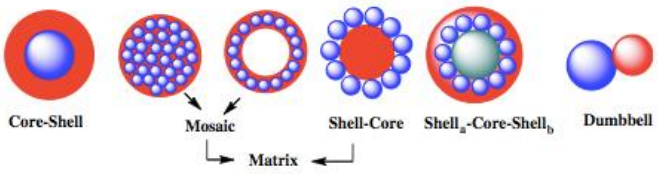

Figure 1.2 Typical structures of MNPs (blue) modified by inorganic materials (red)

[Used from Ref 8 with permission of Springer]

In this thesis, a synthetic polymer PAA was selected as the stabilizer (or the coating agent) due to its exceptional hydrophilicity and its high amount of carboxyl functional groups, which can provide negative charges and therefore electrostatic repulsion between particles in a neutral aqueous system. PAA molecules were also expected to endure the high temperature conditions experienced during the hydrothermal synthesis due to the robustness of a synthetic polymer.

1.4 Applications of Magnetic Nanoparticles

The unique properties of MNPs enable them to be used in a wide range of applications, varying from magnetic resonance imaging (MRI) and hyperthermia creation in bio-medical field [17, 32, 37, 38], pollutants removal in environmental remediation [21], to enzyme immobilization [39, 40], protein purification [41, 42], and pathogen (or toxin) separation in food processing and food safety analysis [19, 43-45].

The application of MNPs to proteins and enzymes immobilization in the food industry has been researched extensively. Food enzymes are vulnerable to rigorous

processing conditions such as extreme pH and high temperature. Covalent immobilization of food enzymes on MNPs not only improves their stability and reusability, but also allows easy separation from the reaction medium and reduces loss of enzymes [43]. Another advantage is the large surface area of MNPs, which provides sufficient space for a high enzyme loading capacity. Some weaknesses of enzyme immobilization are the altered enzyme conformation and thus slightly declined enzymatic activity after immobilization, and the safety concerns regarding the involved MNPs. Nevertheless, many food enzymes such as α-amylase and cellulase have been immobilized on such MNPs supports and were reviewed in literature [43].

Also worth mentioning is the application of MNPs for pathogen capture and detection in food safety analyses. With the rapid development of food industry during the past few decades, foodborne diseases are of great concern to public health. They have also drawn the attention of the food industry as well as consumers. According to Centers for Disease Control and Prevention (CDC), foodborne diseases account for estimated 48 million illnesses, 3000 deaths, and an expenditure of 5 to 6 billion dollars each year in the United States. MNPs have been studied as a promising immunomagnetic separation (IMS) tool for pathogen isolation. By conjugating pathogen antibodies with MNPs and then contacting with pathogen-contaminated samples, efficient capture, concentration, and separation of the foodborne pathogens can be achieved by simply applying an external magnetic field [19, 46-48]. Additional novel analyses can be subsequently conducted on the isolated foodborne pathogens,

such as measuring impedance change [47] and redox activities [49], which are much faster than the classical plating method.

1.5 Study Goal

This study was focused on synthesizing MPs of various sizes, which were less prone to aggregation while maintaining excellent magnetic properties. Despite surface modifications using different types of polymers are widely researched, the effect of a polymer with different Mw on the in situ formed particles has rarely been reported. In addition, polymer-coated MPs synthesized via different synthesis procedures are seldom compared. The varying size and characteristics of the as-synthesized particles could impact their further applications. It was necessary to explore various synthesis methods that produce MPs with different sizes and properties. Furthermore, a lot of literature focused on the synthesis of MNPs of very small size down to a few nanometers, leaving the ease to magnetically separate and collect these MNPs unevaluated. The fastidious synthesis procedure of those very small MNPs may have compromised their magnetic properties. Also, smaller MNPs experience weaker magnetic response to an external magnetic field due to their smaller magnetic cores. Moreover, since a lot of MNPs applications are based on an aqueous system, the thermal motion of these MNPs and the viscous nature of the surrounding water may further impede their movement in water and weaken their magnetic response. These factors can result in difficult collection and manipulation of these MNPs after they are suspended in water.

In this study, Fe_3O_4 MPs coated by PAA with different Mw (1.8K, 30K, 50K, and 100K g/mol) were synthesized using three different hydrothermal approaches, in

order to improve their water dispersibility and versatility. The effects of PAA Mw as well as different synthesis procedures on the size, morphology, magnetic properties, and magnetic collection efficiency of the resulting particles were investigated. The hydrodynamic size, morphology, structure, and the identity of the resultant MPs were characterized by dynamic light scattering (DLS), scanning electron microscope (SEM), transmission electron microscopy (TEM), and x-ray diffraction (XRD), respectively. The magnetic properties of these MPs were characterized by vibrating sample magnetometer (VSM). The amount of PAA bound to the MPs was quantified by thermogravimetric (TG) analysis. The aqueous dispersibility of the synthesized MPs as well as their magnetic collection efficiency from water was also evaluated. Three potential applications of the synthesized PAA-MMPs, namely, food proteins and enzymes immobilization, antibody conjugation for pathogen capture, and magnetic hydrogel film fabrication, were studied.

Chapter 2: Materials and Methods

2.1 Synthesis of PAA-coated Magnetic Particles

2.1.1 One-step Hydrothermal Synthesis

2.1.1.1 Synthesis of PAA-MMPs via one-step hydrothermal procedure

Poly (acrylic acid) (PAA) of four different molecular weights (Mw) were used (1.8K, 30K, 50K, and 100K g/mol). First, 1.5 g PAA was added in the corresponding amount of water and placed on a magnetic stirrer. After stirring the solution for 5 min, 0.2 g ferric ammonium citrate powder (Spectrum Chemical Mfg. Corp.) was added into the solution and stirred vigorously until the powder dissolved. Then 4 ml hydrazine monohydrate (98+%, Alfa Aesar) was added in the solution, one drop at a time. The final volume of each resulting solution was 20 ml, with a PAA mass concentration of 7.5% (w/v). The solution was stirred until homogeneous before being transferred to a 20 ml Teflon-lined stainless-steel autoclave reactor (CIT-HTC230-V25, Col-Int Tech) and maintained at 180°C for 10 h. The solution was cooled to room temperature, and the particles were collected by applying a magnet to the wall of the container. The collected particles were washed with water and ethanol several times respectively before they were dried in air for a few days. PAA (Mw of 1.8K, 30K, and 50K g/mol) were purchased from Polysciences, Inc., and PAA (Mw of 100K g/mol) was purchased from Sigma-Aldrich. All reagents were of analytical grade. The as-synthesized particles will be referred to as PAA-1.8K MMPs, PAA-30K MMPs, PAA-50K MMPs, and PAA-100K MMPs, respectively.

2.1.1.2 Synthesis of bare MNPs without PAA via one-step hydrothermal procedure

The synthesis procedure was the same as the above mentioned, but no PAA was added in. The as-synthesized particles will be mentioned as bare MNPs.

2.1.2 Two-step Hydrothermal Synthesis

The preparation of reactant solution was the same as the one-step hydrothermal route. However, after the solution was transferred to the reactor, it was first maintained at step 1 temperature (100°C or 110°C or 120°C) for 10 h (step 1 time). Then the solution was maintained under room temperature for three days, before it was heated again at step 2 temperature (180°C or 190°C) for another 5 h (step 2 time). The resulting particles were collected by applying a magnet to the wall of the container, and washed with water and ethanol several times respectively, before being dried in air for a few days. The as-synthesized particles will be referred to as PAA-1.8K MNPs, PAA-30K MNPs, PAA-50K MNPs, and PAA-100K MNPs, respectively.

MNPs without PAA were also synthesized via this two-step hydrothermal procedure, with 0, 2, 5, 15 days in between the two heating steps, respectively.

2.1.3 Room-temperature Coating Bare MNPs

Bare MNPs were first synthesized following the procedure described in section 2.1.1.2. After a dry sample was obtained, 3 mg of the powdered particles were first dispersed in 0.6 ml phosphate buffered saline [PBS buffer (0.003 M phosphate, pH 6, 0.1 M NaCl)] and sonicated (Branson B5510 Ultrasonic Cleaner) until they were dispersed well. The coating of PAA on bare MNPs was achieved using 1-ethyl-3-(3-(dimethylamino)propyl) carbodiimide (EDC) (> 98.0%, Tokyo Chemical Industry

Co., Ltd.), which is a carboxyl-to-amine cross-linker. The reaction mixture was again sonicated for 15 min after 0.5 ml EDC solution (0.025 g/ml in PBS buffer) was added in. Finally, 0.5 ml PAA solution (60 mg/ml in PBS buffer) was added in the reaction mixture, followed by sonication and shaking for 30 min. The resulted particles were collected by applying a magnet to the wall of the container, and washed with PBS buffer and water for several times respectively. Then these particles were dried in air for a few days.

2.2 Characterization of PAA-coated Magnetic Particles

2.2.1 Dynamic Light Scattering (DLS)

The hydrodynamic particle size was measured by dynamic laser scattering (DLS) using a BI-200 SM Goniometer Version 2 (Brookhaven Instrument Corp., Holtsville, NY, USA). DLS measurements were conducted using a 35 mW He−Ne laser beam at a wavelength of 637 nm and a scattering angle of 90° at 25°C for 1 min. Refractive index used was 2.42 as around 90% of the particles were composed of Fe_3O_4, evidenced by XRD and TG analysis. The average size was calculated using the intensity of the scattered light and the BIC Dynamic Scattering Software (Brookhaven Instrument Corp., Holtsville, NY, USA).

2.2.2 Scanning Electron Microscopy (SEM)

Scanning electron microscopy (SEM) images were obtained using a Hitachi SU-70 SEM microscope. SEM samples were prepared by suspending and sonicating 1 mg as-synthesized particles in 10 ml water until there is no obvious aggregate. Then 35 ul of the particle suspension was dropped on a 1-inch specimen stub with attached

conductive carbon tape (Electron Microscopy Sciences) and dried in air overnight. The sample was then coated with a thin layer of gold and platinum using a sputter coater (Hummer XP) before obtaining SEM images. Size of particles in dry state was obtained by measuring 30 or above randomly selected individual particles shown in SEM images.

2.2.3 Thermogravimetric (TG) Analysis

To estimate the amount of PAA on 1 mg particle, PAA-MMPs formed via one-step hydrothermal procedure were chosen to perform the TG analysis with a Shimadzu TGA-50 thermogravimetric analyzer. The measurements were conducted in static air at a heating rate of 10°C/min rising from room temperature to 400°C. The samples were oxidized and turned into brownish-red after the measurements. The amount of PAA on 1 mg particle was calculated based on the sample weight loss and the reaction equation of oxidation.

2.2.4 Magnetic Properties

The magnetic properties of all as-synthesized particles were determined by a vibrating sample magnetometer (VSM, 7400, LakeShore Cryotronics, Inc.). Around 10 mg of the powdered particle of each sample was filled into a Kel-F sample holder cup for measurements. The hysteresis loops were obtained by scanning the field intensity from 10 to -10 kOe. All measurements were performed at 25°C.

2.2.5 X-ray Diffraction (XRD) Analysis

Bare MNPs, PAA-50K, and PAA-100K MMPs were used to conduct XRD analysis in order to confirm their identity. The XRD measurements were carried out on a Bruker D8 diffractometer with Cu k-alpha radiation.

2.3 Magnetic Collection of PAA-coated Magnetic Particles in Water

First, 5 g of each PAA-coated MPs (including particles synthesized via all three hydrothermal procedures) were suspended in 10 ml water, respectively, followed by sonication for 5 min or until homogeneous suspensions were obtained. Representative images of the suspensions were taken at this time. Second, a small magnet was applied on the sidewall of the transparent vial of each suspension to collect PAA-coated MPs. The particles were sequentially collected at 10 min, 12 h, and 24 h, after which they were measured and compared to the original total amount, expressed as collected percentage. Representative images of all the suspensions at these time points were also taken.

2.4 Applications of PAA-coated Magnetic Particles

2.4.1 Immobilization of Food Proteins and Enzymes

BSA (98-99%, Sigma) and lysozyme (≥ 90%, Sigma) were chosen to conduct conjugation experiments. Bare MNPs, PAA-1.8K, PAA-30K, PAA-50K, and PAA-100K MMPs were used. The conjugation was performed in 2-(N-morpholino)-ethanesulfonic acid (MES buffer) (Amresco, Inc., Solon, OH) buffer through EDC crosslinking. First, 3 mg particles, 1.8K μl MES buffer (50 mM, pH 4.7), and 210 μl EDC solution (200 mg/ml in pH 4.7 MES buffer) were mixed and sonicated for 15

min, followed by shaking for another 15 min. Next, the particles were separated by applying a magnet to the wall of the container, and the remaining solution was pipetted away. Then 3 ml of a protein solution (3 mg/ml in 50 mM pH 7.0 MES buffer) were added, followed by immediate sonication for 10 min to re-disperse the particles in protein solution. The mixture was then shaken for 50 min. The resulting particle-protein conjugates were separated from the liquid magnetically, and the concentration of the remaining protein solution was determined by measuring its absorbance at 280 nm with a DU-730 UV/VIS spectrophotometer (Beckman Coulter Inc., Fullerton, CA, USA).

2.4.2 Conjugation with Antibody and Capture of *Escherichia coli (E. coli)*

PAA-30K MMPs synthesized via one-step hydrothermal procedure was chosen to covalently conjugate with anti-*E. coli* IgG (1 mg/ml, Thermo Scientific Pierce, IL). The conjugation of anti-*E. coli* to PAA-30K MMPs was achieved via the carboxyl activating agent EDC (0.2 mg/μl). Firstly, 0.9 mg PAA-30K MMPs and 70 μl EDC were mixed in 300 μl MES buffer (50 mM, pH 5.2), sonicated, and shaken at intervals for 30 min, after which the activated PAA-30K MMPs were magnetically separated from the solution and collected to the wall of container. The activated PAA-30K MMPs were then re-suspended in 50 μl MES buffer (50 mM, pH 7.0) and mixed with 50 μL of anti-*E. coli* solution (0.5 mg/mL in pH 7.0 MES buffer) and shaken at 25°C for 1 h. Lastly, the resulting PAA-MMPs-antibody conjugates were again magnetically separated and re-suspended in MES buffer (50 mM, pH 7.0). The PAA-MMPs-antibody conjugates were then mixed with red fluorescing wild-type *E. coli*

W3110 and shaken for 15 min, before they were magnetically separated and washed with MES buffer.

2.4.3 Fabrication of Magnetic Hydrogel Films

The chemicals used in this section were purchased from Sigma-Aldrich, including chitosan from crab shells (85% deacetylation and 200 kDa), KH_2PO_4, K_2HPO_4, pyrocatechol, ascorbic acid, 1,1'-ferrocenedimethanol (Fc, 97%), and pyocyanin from *Pseudomonas aeruginosa* (PYO, ≥98%).

2.4.3.1 Preparation of Chitosan Solution

To make 500 ml chitosan solution (1%, pH 5.3), 5 g or slightly more of chitosan was first added in 200 ml distilled water. The pH of solution was then adjusted to 5.3 with 1 M HCl, followed by constantly stirring for 2-4 h and occasionally monitoring the pH value. When there was minimal amount of insoluble matter seen visually, the chitosan solution was filtrated through a coarse filter (metal mesh) under vacuum. The resulting solution was filtrated again through a Busher funnel (pore size of 40 μm) under vacuum. The concentration of this final chitosan solution was measured and diluted to 1% as needed.

2.4.3.2 Electrodeposition of Chitosan-MMPs Films and Electrochemical Modification

First, 3 mg of PAA-100K MMPs was suspended in 1 ml chitosan solution (1%, pH 5.3), which was then sonicated and shaken for 15 min. An electrodeposition device was assembled by placing a Teflon cylinder container with a hole (8 mm in diameter) on a piece of 10 mm x 20 mm gold wafer as the cathodic electrode. The electrodeposition process was achieved by connecting the electrodes to a DC power source (2400 Sourcemeter, Keithley Instruments, Inc.), which provided a constant

current density of 3 A/m^2 to the gold electrode. A 300 μl 1% chitosan solution was first added into the hole on top of the gold wafer electrode, and a Pt wire as the anodic electrode was immersed into the solution. Electrodeposition of chitosan lasted for 1 min. After rinsing the deposited film with buffer and drying it in the air, 300 μl chitosan-MMPs suspension (3 mg MPs/ml) was added, followed by placing a magnet (field strength of 0.7 kOe) under the solution for 5 min and then electrodeposition for another 3 min. The extra chitosan-MMPs suspension was removed, and the deposited chitosan-MMPs film was gently rinsed with distilled water and phosphate buffer (PB buffer) 2-3 times followed by drying it in the air.

Second, the deposited chitosan-MMPs film was electrochemically modified with catechol by immersing the film in 3 ml catechol solution (10 mM, 0.1 M phosphate buffer, pH 7.0). An anodic potential (+0.5 V, 60s) was applied using a three-electrode system through a CHI Instruments 6273C electrochemical analyzer (CH instruments, Inc., Austin, TX), with the gold electrode as a working electrode, Pt wire as a counter-electrode, and Ag/AgCl as a reference electrode. The oxidation products from catechol hence grafted to chitosan-MMPs films.

2.4.3.3 Cyclic Voltammograms

The cyclic voltammogram (CV) of the catechol-grafted chitosan-MMPs film (cat-chit-MMPs film) was carried out using the CHI 6273C electrochemical analyzer. The same three-electrode system as the modification process in section 2.4.3.2 was applied. The film was first immersed with only one mediator Fc (50 μM, PB buffer 0.1 M, pH 7.0) to discharge the film, and the applied potential was swept from 0 V to

+0.5 V with a scan rate of 0.05 V/s. Then the film was immersed by 5 mM ascorbic acid for 5 min to re-charge the film, before replacing with Fc again.

The cat-chit-MMPs film was then immersed in solution containing both redox mediators (Fc and PYO, 50 μM, PB buffer 0.1 M, pH 7.0), to repeatedly discharge and re-charge the film. The applied potential was swept continuously from −0.4 V to +0.5 V with a scan rate of 0.05 V/s.

2.5 Statistical Analysis

T-test statistical analysis with a confidence level of 95% was conducted to achieve pairwise comparison of the size of PAA-coated MPs.

Chapter 3: Results and Discussion

3.1 Effect of Synthesis Procedures on Particles' Size and Morphology

Syntheses of PAA-coated MPs using different Mw of PAA and via three different hydrothermal procedures were performed in order to compare the resulting particle size and morphology. The three hydrothermal procedures were one-step hydrothermal, two-step hydrothermal, and room-temperature coating bare MNPs, respectively.

3.1.1 One-step Hydrothermal Synthesis

Effect of PAA Molecular Weight

PAA with Mw of 1.8K, 30K, 50K, and 100K g/mol were chosen to obtain PAA-MMPs via one-step hydrothermal procedure to investigate the effect of Mw on particle size and morphology. PAA mass concentration was controlled to be 7.5% for all treatments. The synthesis temperature involved was 180°C. The hydrodynamic particle size was characterized by DLS, denoted as hydrodynamic diameter (D_H). The morphology of the dried particles was observed under SEM at different magnifications, from which their size was also measured. As shown in Figure 3.1, the use of PAA in particles synthesis dramatically increased the D_H of the resulting particles. In addition, as the PAA Mw increased from 1.8K to 100K g/mol, the D_H of the particles decreased from 2527.2 nm to 258.4 nm with narrower size distribution. Similarly, Figure 3.2 (a) to (d) showed much larger sizes of the PAA-MMPs than the bare MNPs in Figure 3.2 (e). The particle size also decreased as the PAA Mw increased. The size measured in SEM was slightly different from DLS for PAA-30K,

PAA-50K, and PAA-100K MMPs, which was because DLS determined the hydrodynamic particle size in water and possibly the size of some aggregates, while SEM images revealed the individual particles in dry state with collapsed PAA layer. The size of PAA-1.8K MMPs determined by DLS was nearly twice as big as that in SEM, which was mainly due to the amorphous structure of PAA-1.8K MMPs and the large aggregates detected by DLS.

SEM images showed that PAA-1.8K MMPs consisted of big and irregular-shaped aggregates, while PAA-30K, PAA-50K, and PAA-100K MMPs were isolated well-shaped spheres. Comparing PAA-1.8K and PAA-100K MMPs, since PAA mass concentration was the same, the PAA Mw could be the reason that resulted in different particle configurations.

It was worth noticing that the particles formed with higher Mw PAA exhibited yellower color (can be seen in Figure 3.9), with PAA-100K MMPs being the yellowest, which were apparently different from the black bare MNPs and PAA-1.8K MMPs. No previous literature was found regarding yellow-brown Fe_3O_4 particles. In order to investigate the identity of these yellow-brown particles and the role that high Mw PAA played in particle formation, PAA-50K and PAA-100K MMPs were selected to perform the XRD measurement, representing the particles formed in a high Mw polymer matrix. XRD was also performed on bare MNPs as a reference, whose formation did not involve polymer, representing the particles formed without a constrained polymer network. The obtained XRD patterns were searched against ICDD powder diffraction database and matched Fe3O4 magnetite phase (PDF no. 01-076-0955), displayed in Figure 3.2 (f). Apparent broadened peaks were observed in

the XRD pattern of PAA-100K MMPs with decreased intensity compared to the other two, suggesting that it has reduced crystallinity of magnetite [6].

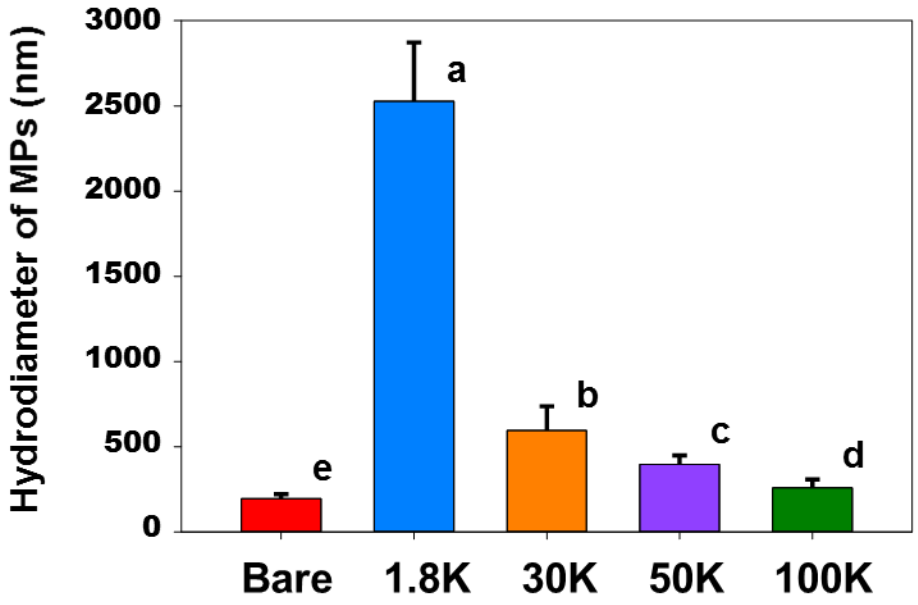

Figure 3.1 DLS characterized hydrodynamic size of one-step hydrothermal synthesized bare MNPs (192.3±22.4 nm), PAA-1.8K MMPs (2527.2±344.9 nm), PAA-30K MMPs (595.5±142.1 nm), PAA-50K MMPs (396.3±51.2 nm), and PAA-100K MMPs (258.4±49.9 nm), respectively.

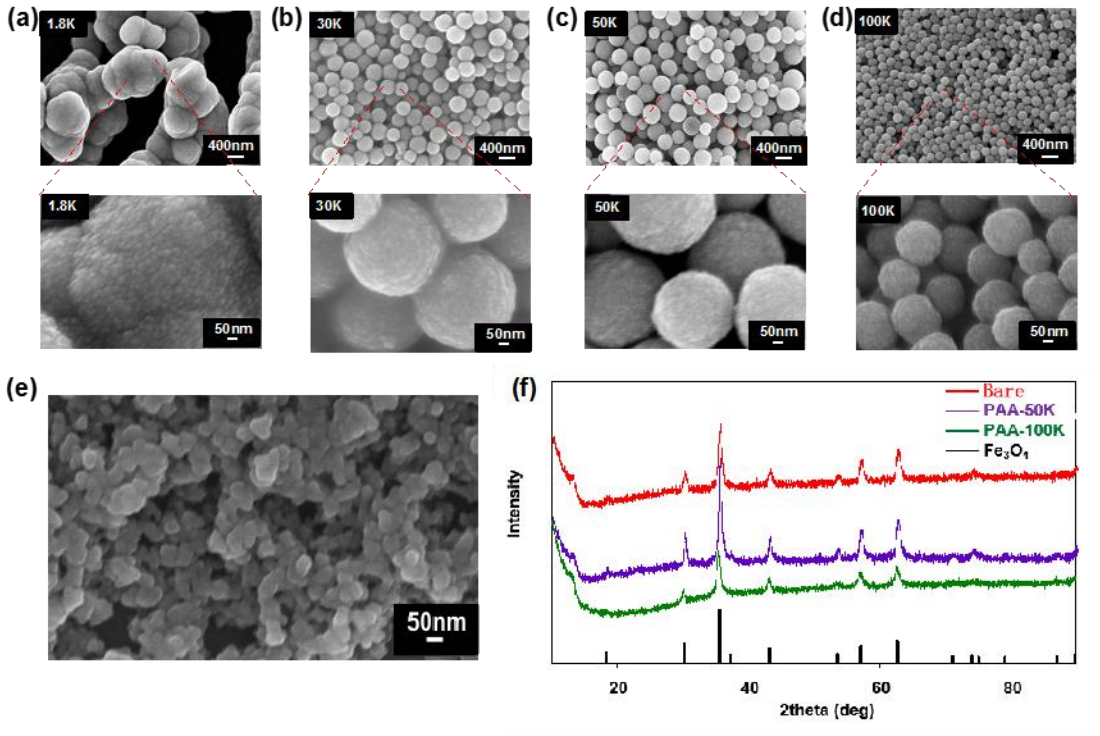

Figure 3.2 SEM images of one-step hydrothermal synthesized

(a) PAA-1.8K MMPs (1201.2±358.6 nm), (b) PAA-30K MMPs (447.3±156.0 nm),

(c) PAA-50K MMPs (417.7±87.7 nm), and (d) PAA-100K MMPs (247.1±33.9 nm),

(e) bare MNPs (66.4±14 nm).

(f): XRD patterns of one-step hydrothermal synthesized bare MNPs, PAA-50K

MMPs, and PAA-100K MMPs.

The crystallite size of these Fe_3O_4 particles was then calculated (Table 3.1) using the Scherrer equation:

$$L = \frac{K\lambda}{\beta cos\theta} \qquad (1)$$

where L is the average crystallite size (nm), K is Scherrer constant related to crystallite shape (K=0.89), λ is the X-ray wavelength (~ 1.5418Å), β is the peak breadth measured at half the maximum intensity (FWHM) (radians), and θ is the Bragg's angle (degrees) [50, 51]. While the absolute crystallite size of one sample determined by Scherrer equation is roughly accurate [52, 53], the difference in relative sizes between two samples is a more meaningful reference. From Table 3.1, PAA-100K MMPs showed a much smaller crystallite size compared to bare MNPs and PAA-50K MMPs. This indicates the PAA with Mw of 100K g/mol could significantly limit the growth of in situ formed primary nanocrystals due to the tougher polymer matrix and thus a constrained environment it offered [54], while still yielding Fe_3O_4 particles but with lower yield. High Mw of PAA may also slowed the nucleation rate of nanocrystals [55], leading to a smaller size of primary nanocrystals.

Table 3.1 Crystallite size of one-step hydrothermal synthesized bare MNPs, PAA-50K MMPs, and PAA-100K MMPs

Samples	Crystallite Size (nm)
bare MNPs	23.7±0.4 [b]
PAA-50K MMPs	24.5±0.3 [a]
PAA-100K MMPs	18.2±0.4 [c]

The formation of Fe_3O_4 MMPs involves both nucleation of nanocrystals and aggregation into bigger secondary structure [56]. The SEM images of PAA-MMPs and

their crystallite size determined by XRD verified that they are large secondary structure comprised of plentiful small nanocrystals. In the current system, the existing PAA backbone could bind to the particles immediately after Fe_3O_4 nucleation to prevent nuclei growth [57]. PAA also participated in the adhesion among primary nanocrystals within the secondary structure [33], which could be testified by the much smaller size of one-step hydrothermal synthesized bare MNPs without PAA (192.3±22.4 nm by DLS and 66.4±14 nm by SEM).

When a particle covered by polymer collided with another particle uncovered by polymer, flocculation occurred and aggregate was formed. The surface in-between these two particles could not be attached by more polymers [58]. When higher Mw polymer was applied, more particles were completely covered as soon as they are formed, since polymer adsorption was faster than flocculation [59]. Therefore, PAA of higher Mw was able to reduce the formation of big aggregates between covered and uncovered particles. Higher Mw PAA also resulted in particles of more uniform size, because the electrostatic repulsion between two polyelectrolytes of same charges could prevent the coalescence of multiple particles [6].

Although all PAA-MMPs contain large secondary aggregates, PAA-1.8K MMPs are particularly sizable, which might be attributed to the relatively low Mw and a different flocculation mechanism of PAA when compared with other treatments.

Previously, PAA has been studied as a flocculant [60]. The flocculation effect of PAA on nucleated Fe_3O_4 nanocrystals could also be evident from representative TEM images of PAA-50K and PAA-100K MMPs, which intended to further explore the substructure of PAA-MMPs. The PAA-MMPs observed in Figure 3.3 (a) and (b)

appeared to be comprised of a large quantity of nanocrystal Fe_3O_4 cores. The density of Fe_3O_4 cores was found higher at the particle boundary than in the center for most of the PAA-MMPs. In addition, the center of PAA-50K MMPs was darker than PAA-100K MMPs, implying a higher percentage of magnetic cores in a single PAA-50K MMP, which might be related to their magnetic property discussed later. The size and morphology of PAA-100K MMPs was more uniform than those of PAA-50K MMPs, corresponding to the DLS measurements conducted before.

The PAA layer adsorbed on PAA-100K MMPs was found much thicker and consistent than PAA-50K MMPs. As shown in Figure 3.3 (a), the PAA layer observed on PAA-50K MMPs varied from 0.6 nm to 0.8 nm. By contrast, the PAA-100K MMPs contained a thicker PAA layer, varying from 4.5 nm to 6.3 nm, according to currently available TEM images.

However, PAA layer less than 1nm thick was hardly to be measured accurately, and the thickness of PAA layer differed from one inspected particle to another. Also, the hollow center of the particles shown in TEM images might or might not contain PAA. Hence, TG analysis was further performed on one-step hydrothermal synthesized PAA-MMPs to quantify their PAA content (Figure 3.3 (c)). There were two falls of the curve in each TG measurement (take PAA-1.8K MMPs as an example), of which the first fall was majorly attributed to the water evaporation, with the second fall attributed to the burning of PAA. The content of PAA on unit weight of particles was simply calculated via equation (2):

$$PAA\ (\%) = \frac{W_i - a \times W_f}{W_f} \qquad (2)$$

where W_i represents the initial weight of a PAA-MMPs sample in TG analysis (between the first and the second curve fall), W_f represents the final weight of the sample after TG analysis, and α is a conversion factor that equals to 0.97. Since the particles were possibly oxidized into Fe_2O_3 (W_f) at high temperature during TG analysis, the conversion factor was adopted in order to calculate a more precise PAA content on the original particles.

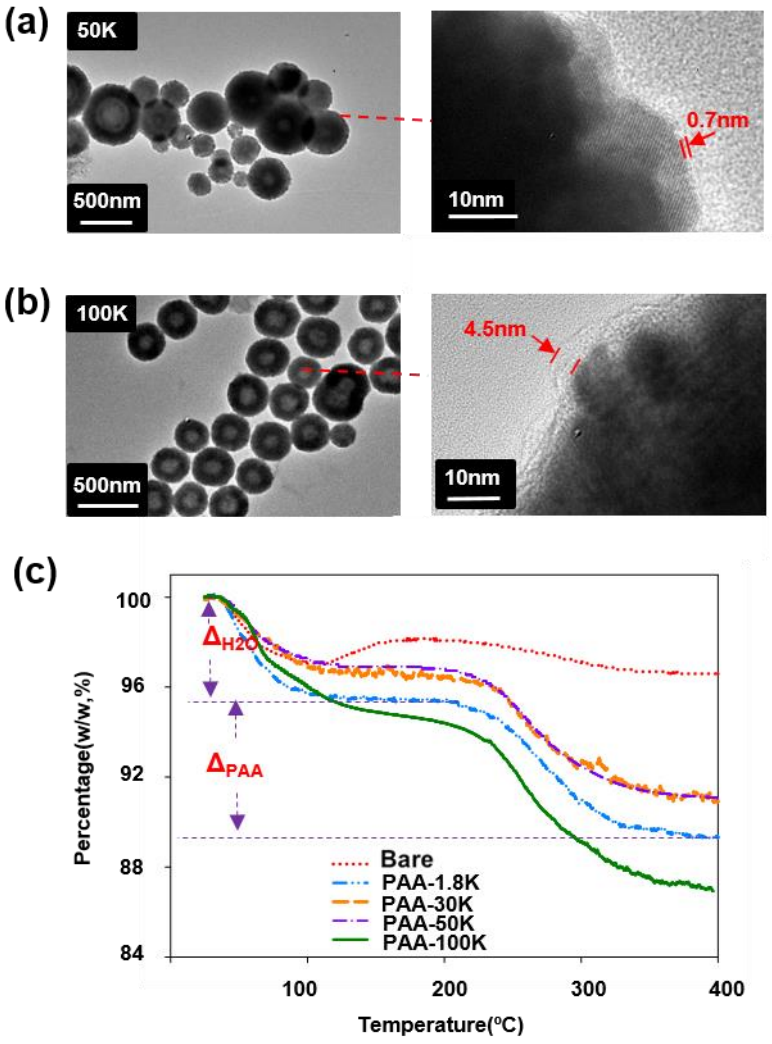

Figure 3.3 Representative TEM images of one-step hydrothermal synthesized (a) PAA-50K MMPs, (b) PAA-100K MMPs.

(c) TG analysis of one-step hydrothermal synthesized bare MNPs and PAA-MMPs.

The amount of PAA on 1 mg of PAA-1.8K MMPs (0.106 mg), PAA-30K MMPs (0.095 mg), and PAA-50K MMPs (0.101 mg) were found to be similar. PAA-100K MMPs was calculated to consist of 0.123 mg PAA per mg particle, 14% more than that of PAA-1.8K MMPs and 18% more than that of PAA-50K MMPs. This corresponded to the preliminary observed TEM images. The large surface area of PAA-100K MMPs due to their relatively small particle size allowed the adsorption of higher amount of polymer compared to others. This corresponds to similar discussion in previous literature, where small particles adsorbed greater amount of polymer [6].

One phenomenon noticed during the preparation of reaction solution was that, when ferric ions and hydrazine were mixed in the presence of PAA, the solution immediately turned black and then green, probably resulting from the reduction of ferric ions. However, when PAA was absent, it took much longer time for the solution turning from black to green. This phenomenon may be attributed to the steric entrapment of ion cations in the PAA entanglement, which limited oxidation of ion cations by ambient oxygen [61].

Effect of Temperature

Besides the Mw of PAA, synthesis temperature was also speculated to affect the size of the as-synthesized particles, based on previous literature [33]. Therefore, PAA-30K MMPs were synthesized via one-step hydrothermal procedure at three different temperatures (160°C, 180°C, 200°C) for 10 h. As shown in the Table 3.2, the D_H of the as-synthesized particles decreased by more than 57.2% as the synthesis temperature increased. The PAA-30K MMPs synthesized at 200°C demonstrated the

smallest size among these three synthesis temperatures. The process of Fe_3O_4 formation may rationalize this size difference.

Table 3.2 Effect of synthesis temperature on the hydrodynamic size of one-step hydrothermal synthesized PAA-30K MMPs by DLS

Reaction temperature (°C)	Reaction time (h)	Particle Size (nm)
160	10	1020.9±61.2 [a]
180	10	589.6±49.1 [b]
200	10	436.9±22.2 [c]

As specified earlier, formation of Fe_3O_4 consisted of two steps. The nucleation of the primary nanocrystals occurred at the first step. Then the primary nanocrystals grow and aggregate into a bigger secondary structure at the second step when the reaction time was elongated. The studied system provided enough time for both steps.

The detailed reaction process has been discussed before in a similar hydrothermal system [55]:

$$3\ N_2H_4 = N_2 + 4\ NH_3 \quad (3)$$

$$NH_3 + H_2O = NH_4^+ + OH^- \ ;\ N_2H_4 + H_2O = N_2H_5^+ + OH^- \quad (4)$$

$$Fe(OH)_3 = FeO(OH) + H_2O \quad (5)$$

$$12\ FeO(OH) + N_2H_4 = 4\ Fe_3O_4 + 6\ H_2O + N_2 \quad (6)$$

The smaller particle size synthesized under higher reaction temperature could be explained via the different rates of nucleation and grain growth. At higher synthesis

temperature, the nucleation rate might be faster than the grain growth [33], which dominated the consumption of reaction solute and possibly postponed the size increase of primary nanocrystals. As a result, the size of secondary structure would be reduced. The larger amount and smaller size of in situ formed primary nanocrystals might also provide greater surface area that allowed PAA molecules to adhere, favoring morphology control and yielding more uniform PAA-MMPs.

3.1.2 Two-step Hydrothermal Synthesis

In two-step hydrothermal route, the reactant solution was first kept at 120°C for 10 h, after which the solution were aged under room temperature for 3 days, followed by being heated at 180°C for another 5 h. PAA of different Mw (1.8K, 30K, 50K, and 100K g/mol) were again added at the beginning as stabilizers for particles, in order to study the effect of PAA Mw in this synthesis procedure. The hydrodynamic particle size was measured by DLS (Figure 3.4), and SEM images of the particles in dry state were taken (Figure 3.5). The synthesis temperature and room-temperature aging time were also tuned to examine their effects on the size of the resulting particles, displayed in Table 3.3 and Figure 3.5.

Effect of Aging Time

Regarding the synthesis of MNPs without PAA, the effect of different aging time under room temperature on the particle size was first examined by observing bare MNPs that underwent 0, 2, 5, and 15 days of room-temperature aging, respectively. As shown in Figure 3.5 (a), no significant difference was found among bare MNPs that experienced different aging times. Therefore, aging time under room

temperature did not have a noteworthy contribution to the size change of the synthesized MNPs.

However, since the size of MNPs from two-step hydrothermal synthesis was much smaller than that from one-step hydrothermal synthesis, the effect of aging time at high temperature might be prominent. It was reported that longer aging time at high temperature assisted in formation of bigger particles by providing enough time for Ostwald ripening, which is the other mechanism of forming large and well-shaped MPs [62-64], in addition to the flocculation effect of PAA. Through precise control of aging process and temperature, the size and morphology of synthesized MPs or MNPs could be effectively adjusted.

Effect of PAA Molecular Weight

DLS measurement in Figure 3.4 showed the hydrodynamic size increase of the particles when PAA was added. Figure 3.5 (b) revealed the size and morphology of the PAA-MNPs when different PAA Mw was used in two-step hydrothermal synthesis. PAA-1.8K MNPs from two-step hydrothermal synthesis were found to be spheres with the smallest size, which seemed to be undergoing the process of forming large and irregular-shaped aggregates. The size of PAA-30K and PAA-50K MNPs was similar. PAA-100K MNPs were smaller then PAA-30K and PAA-50K MNPs, while larger than single spheres of PAA-1.8K MNPs. Although all of these MNPs were much smaller than the corresponding MMPs from one-step hydrothermal procedure, the effect of PAA Mw could still be roughly estimated. The highly constrained polymer network provided by PAA-100K limited the growth of spherical MNPs aggregates, while the weaker polymer matrix of PAA-1.8K possibly

contributed to the amorphous aggregates structure with high amount of single nanocrystals.

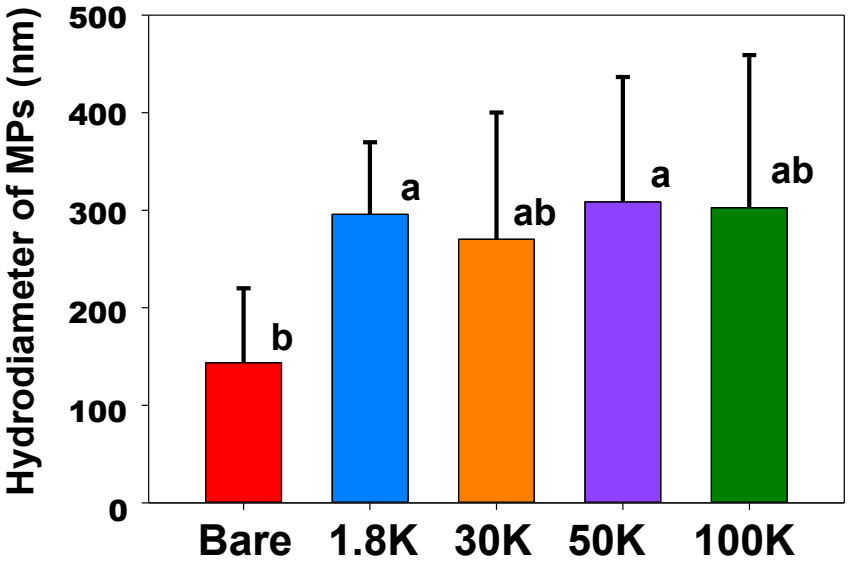

Figure 3.4 DLS characterized hydrodynamic size of two-step hydrothermal synthesized bare MNPs (143.6±76.4 nm), PAA-1.8K MNPs (295.98±73.8 nm), PAA-30K MNPs (270.35±129.8 nm), PAA-50K MNPs (308.64±128.1 nm), and PAA-100K MNPs (302.8±156.2 nm), respectively (room-temperature aging time=3 days).

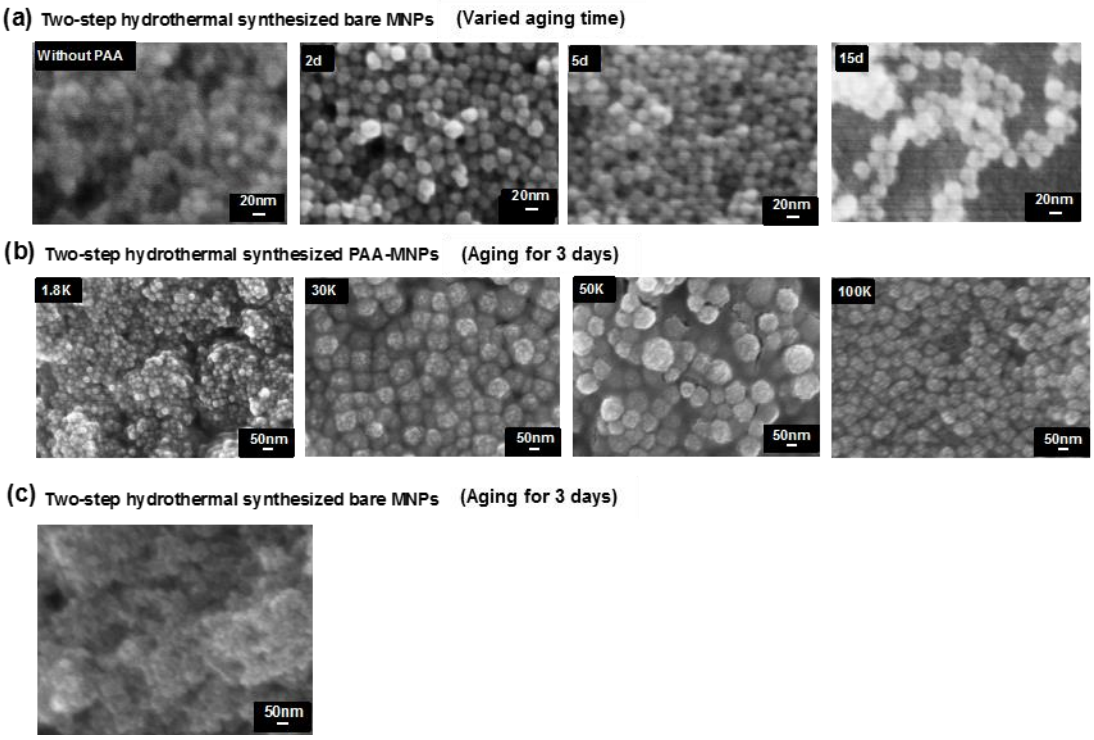

Figure 3.5 SEM images of two-step hydrothermal synthesized (a) bare MNPs under varied room-temperature aging time [left to right: 0 day (22±2.9 nm), 2 days (23±3.2 nm), 5 days (22.6±3.4 nm), and 15 days (25.5±2.7 nm)]; (b) left to right: PAA-1.8K MNPs (33±2.9 nm), PAA-30K MNPs (100±14.1 nm), PAA-50K MNPs (115.6±25.9 nm), and PAA-100K MNPs (77.6±6.4 nm). (c) bare MNPs under room-temperature aging time of 3 days (27.8±4.2 nm).

Effect of Temperature

Two-step hydrothermal synthesis procedure included step 1 and step 2 temperatures, which may or may not have the same effect on the formation of PAA-MNPs. Therefore, four different combination of step 1 and step 2 temperatures were designed to investigate whether both temperatures could affect the size of synthesized PAA-30K MNPs (Table 3.3). The first 10 h heating at 120 °C caused the color of

solution changing from green to dark red with some amount of collectable black particles. The following 5 h heating at 180°C allowed the production of more collectable particles within shorter time. As shown in Table 3.3, step 1 temperature did not demonstrate a clear relationship with the PAA-30K MNPs size ($P > 0.05$); instead, step 2 temperature might have more impact on the resulting particle size, when comparing the third and the fourth trial in Table 3.3. It was suspected that the effect of step 2 temperature on particle size was similar to that in one-step hydrothermal procedure. The size difference between DLS and SEM measurement has been discussed earlier, which was primarily attributed to the aggregated particles detected by DLS.

Table 3.3 The effect of temperature on particle size of PAA-30K MNPs in two-step hydrothermal procedure by DLS

Step 1 Temp. (°C)	Step 1 Time (h)	Aging time (days)	Step 2 Temp. (°C)	Step 2 Time (h)	Particle Size (nm)
100	10	3	180	5	438.9±34.3 [ab]
110	10	3	180	5	491.1±71.2 [a]
120	10	3	180	5	467.5±26.7 [a]
120	10	3	190	5	349.4±81.3 [b]

3.1.3 Room-temperature Coating Bare MNPs

Besides the above two synthesis procedures, a third synthesis procedure was also conducted using PAA with different Mw (1.8K, 30K, 50K, and 100K g/mol) to compare the effect of PAA Mw on the D_H of the resulted PAA-MNPs. In this synthesis procedure, bare Fe_3O_4 MNPs without PAA were first synthesized, after which PAA with different Mw was covalently coated onto the bare MNPs via EDC crosslinking. PAA mass concentration was controlled to be 1.88% for all Mw. The D_H of the as-synthesized particles was measured by DLS.

In contrast to one-step hydrothermal procedure, where the higher Mw yielded particles with smaller size (Figure 3.1), a different phenomenon was presented in this synthesis route (Figure 3.6). As the PAA molecular weight increased from 0 to 50K g/mol, the D_H of MNPs increased from 192.3 nm to 500.0 nm. However, instead of continuing the trend to have an expected bigger D_H, PAA-100K MNPs was around 460.6 nm. Statistical analysis also demonstrated that there was no significant difference among the D_H of MNPs coated by PAA with Mw of 30K, 50K, and 100K g/mol. The difference in the size trend between this synthesis and the one-step hydrothermal synthesis could be attributed to absorption of PAA on particles. In one-step hydrothermal synthesis, the Fe_3O_4 nanocrystals were nucleated in situ in the presence of higher amount of PAA, which provided a highly constrained network and helped flocculation of nanocrystals immediately after nucleation. The nanocrystals could be nucleated inside as well as outside a PAA molecule. However, in this synthesis procedure, the Fe_3O_4 nanocrystals were first synthesized and subjected to PAA coating sequentially, where the gyration radius, molecule configuration, and the

concentration of PAA would have a large impact on the resulting PAA-MNPs size. PAA with higher Mw had a bigger gyration radius [65], but mostly smaller than the size of Fe_3O_4 nanocrystals. Therefore, the PAA molecules were conjugated or absorbed only on the surface of nanocrystals. As the Mw of PAA increased, the size of resulted PAA-MNPs increased. PAA with higher Mw occupied more space and posed steric hindrance for other PAA molecules, so the size of the resulting PAA-MNPs was not able to rise infinitely but instead reached saturation. Limited absorption of polymer with high Mw was also reported elsewhere [59].

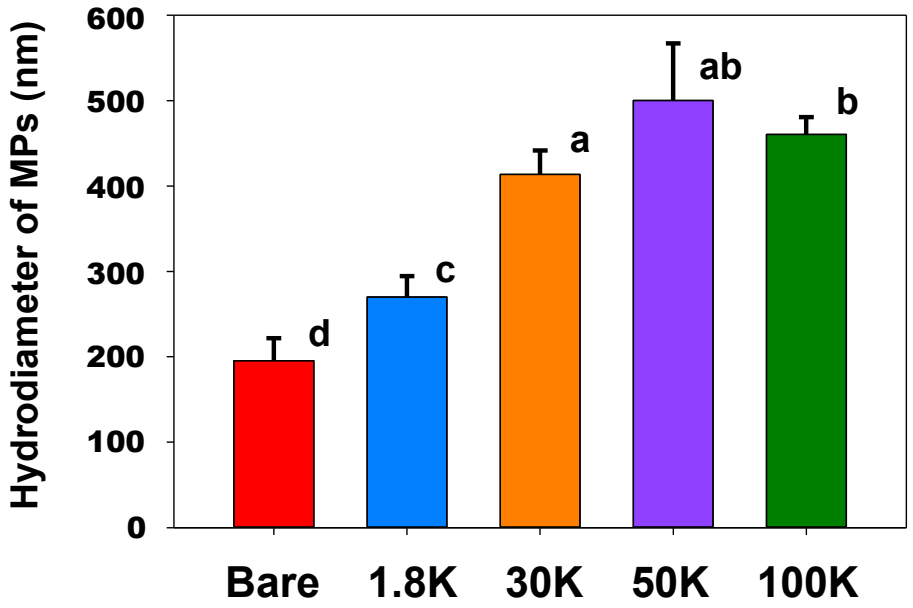

Figure 3.6 DLS characterized hydrodynamic size of MPs from room-temperature coating procedure: bare MNPs (192.3±22.4 nm), PAA-1.8K MNPs (270.3±24.3 nm), PAA-30K MNPs (413.7±28.0 nm), PAA-50K MNPs (500.3±66.9 nm), and PAA-100K MNPs (460.6±20.2 nm).

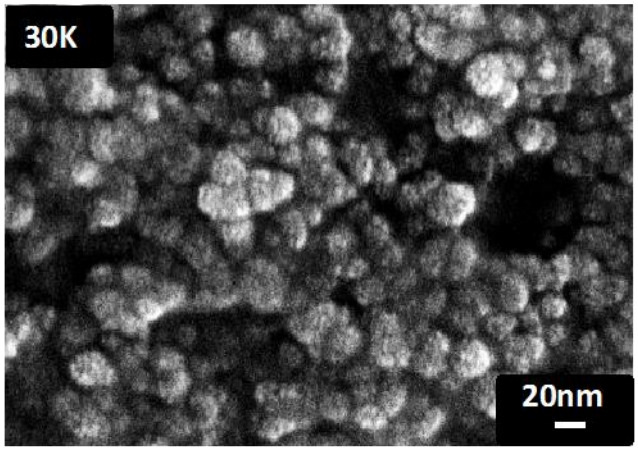

Figure 3.7 SEM image of PAA-30K MNPs obtained from room-temperature coating procedure (30.8±4.3 nm).

3.2 Magnetic Properties of PAA-coated Magnetic Particles

In order to understand the magnetic properties of the synthesized PAA-MMPs and PAA-MNPs, the particles from all three syntheses were subjected to magnetic properties measurement using VSM. A typical hysteresis loop of PAA-MMPs formed via one-step hydrothermal procedure was shown in Figure 3.8 (a), which also revealed the remanent magnetization (M_r), saturation magnetization (M_s), and coercivity (Hc) of this sample. The M_r, M_s, and Hc of all the samples are also shown in Figure 3.8 (b) to (e). M_s indicates the maximal magnetization of the material that can be reached by increasing the applied external magnetic field. M_r implies the magnetization that can be remained after the M_s is reached and the external magnetic field is removed. Hc represents the required intensity of the external magnetic field to bring the magnetization of the material back to zero after M_s is reached. Squareness

ratio (M_r/M_s) provides information about how square a hysteresis loop is and the super-paramagnetism of a material.

For PAA-MMPs formed via one-step hydrothermal procedure, the M_r of PAA-1.8K, PAA-30K, and PAA-50K MMPs was all around 4 emu/g, nearly one-fold higher than bare MNPs and PAA-100K MMPs. The M_r may explain the varying speed when collecting particles, which potentially affects their further applications in terms of efficiency. Although the difference of one-step hydrothermal synthesized samples in M_s was much smaller, the M_s of bare MNPs was the highest (70.3 emu/g) among all samples, indicating that the formation of PAA-MMPs via this procedure slightly decreased their M_s. This could be explained by two reasons. On one hand, the non-magnetic PAA coating reduced the fraction of pure Fe_3O_4 magnetic cores and reduced its magnetic moment per unit mass of particle. On the other hand, for small MNPs crystals, the existence of disordered spin configuration near particle surface may also result in reduced magnetization compared to the corresponding bulk materials[1, 2, 66, 67]. Furthermore, it was shown in the TEM images (Figure 3.3) that the center of one-step hydrothermal synthesized PAA-50K MMPs was denser than PAA-100K MMPs, which suggested that the magnetic cores occupied a higher percentage in a single PAA-50K MMPs. The TEM images thus assisted in explaining the higher M_r and M_s of unit mass of PAA-50K MMPs compare to PAA-100K MMPs in the VSM measurements. The highest Hc was achieved by PAA-1.8K MMPs (35.8 Oe) and lowest by PAA-100K MMPs (10.9 Oe), more than two-thirds less than the former. The squareness ratio of PAA-1.8K, PAA-30K, and PAA-50K MMPs were around 0.06, which were two to three-fold higher than PAA-0 and PAA-100K MMPs.

For PAA-MNPs formed via two-step hydrothermal procedure, the M_r of PAA-30K and PAA-50K MNPs was about 6.3 emu/g, which is much higher than the other samples. This may be due to the more ordered magnetic structure within these particles. M_s of samples were similar (~ 69.0 emu/g), with the exception of PAA-100K MNPs (61.6 emu/g). Hc of PAA-0, PAA-30K, and PAA-50K MNPs were about three-fold higher than PAA-1.8K, and about five-fold more than PAA-100K MNPs. This showed that the inner magnetic structure among nanocrystals might be different. Comparing particles synthesized via one-step and two-step hydrothermal procedures, the different aging time both under room temperature and the synthesis temperature may probably contribute to their crystallinity, particle size, and thus different magnetic properties [68]. The squareness ratio of PAA-1.8K and PAA-100K MNPs (~ 0.020) was much smaller than the other samples from this synthesis procedure, which also indicated different inner magnetic structure might be present.

For PAA-MNPs formed via room-temperature coating procedure, the resulted MNPs demonstrated decreasing M_r from 2.3 emu/g to 1.9 emu/g as the PAA Mw increased. M_s of bare MNPs (70.3 emu/g) was slightly higher than the rest, which were all around 57.0 emu/g. Hc of bare MNPs (20.6 Oe) was also slightly higher than other, which were about 17.5 Oe. Nevertheless, the difference here was small compared to that of the other synthesis procedures, which implied that this synthesis procedure did not greatly affect the magnetic properties of the resulting PAA-MNPs. Their magnetic properties may mainly be determined by that of the selected initially bare MNPs before coating. The slightly lower M_r, M_s, and Hc of MNPs after PAA

coating process could be ascribed to the introduction of non-magnetic material. The squareness ratio for all samples via this synthesis procedure was around 0.035.

It is worth noticing that low Hc (~10 oe) and small squareness ratio (~0.02) indicated the transition from ferromagnetic to super-paramagnetic, which was a size effect present in single-domain crystallites [69]. Therefore, PAA-100K MMPs from one-step hydrothermal synthesis, PAA-1.8K MNPs, and PAA-100K MNPs from two-step hydrothermal synthesis exhibited apparent super-paramagnetic behavior with high M_s, low Hc, and small squareness ratio. For instance, the squareness ratio of PAA-100K MMPs from one-step hydrothermal synthesis was 0.02, meaning that the particles will lose more than 98% of its magnetism when the external magnetic field is removed. Super-paramagnetic particles have low aggregation tendency due to high M_r and thus magnetic interaction. At the same time, they could have high magnetic response when an external magnetic field is applied.

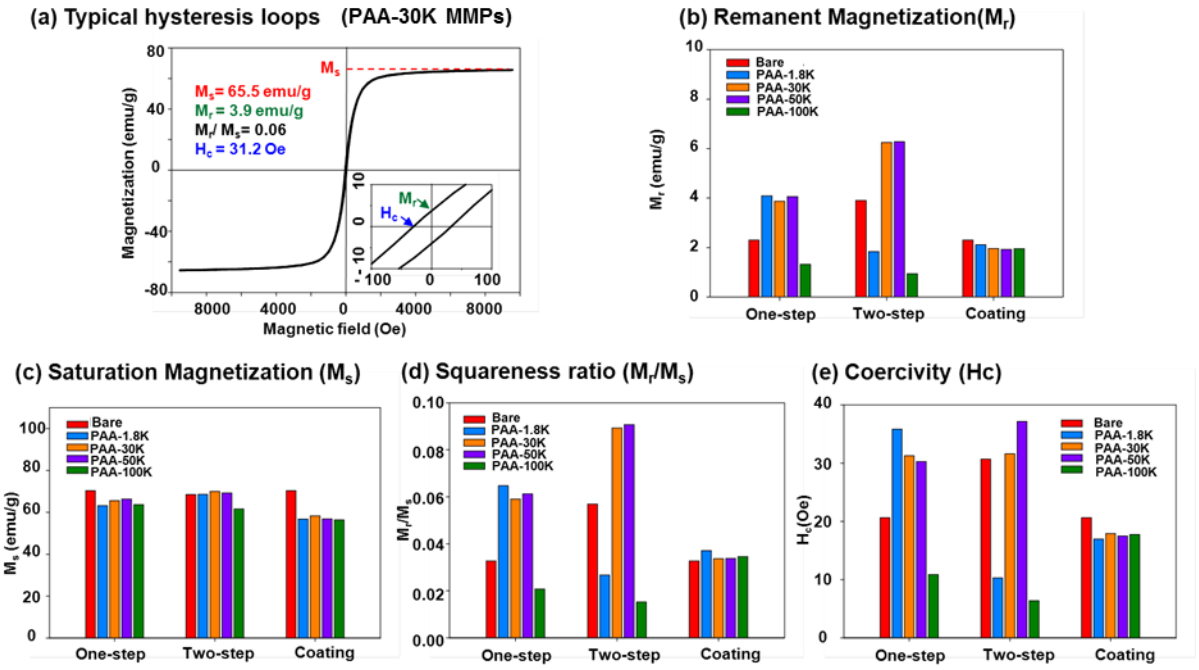

Figure 3.8 (a) Typical hysteresis loop of PAA-MMPs formed via one-step hydrothermal procedure. Magnetic parameters of particles formed via three syntheses: (b) remanent magnetization (M_r), (c) saturation magnetization (M_s), (d) squareness ratio (M_r/M_s), and (e) coercivity (Hc).

3.3 Magnetic Collection of PAA-coated Magnetic Particles in Water

VSM measurement revealed the magnetic properties of dried MPs. However, MPs are usually suspended and applied in an aqueous system, which is the basis of a lot of bio-applications. The movement of these suspended MPs in water upon applying an external magnetic field may be influenced by other factors in the system besides their magnetic properties in the dry state. The speed of the movement of these MPs in water is of significance regarding their collectability and reusability in latent applications. Therefore, the magnetic collection efficiency of the as-synthesized MPs in water was also studied. The left side of Figure 3.9 showed the pictures of MPs suspensions before and after a small magnet has been applied on the sidewall for 10 min, 12 h, and 24 h, respectively. The right side of Figure 3.9 shows the graphs comparing the collected percentage of the MPs after 10 min, 12 h, and 24 h of an external magnet application respectively. PAA-MMPs formed via one-step hydrothermal synthesis procedure (except bare MNPs) were collected at the fastest speed, which were collected 100% or near 100% within the first 10 min (Figure 3.9 (a)). This suggested that the fast movement of these PAA-MMPs in water and high magnetic response when an external magnetic field was applied, which could be due to the large secondary structure and big particle size. PAA-MMPs from this synthesis also exhibited the best water dispersibility, since it took less than 2 min to suspend the

particles thoroughly in water, compared to more than half an hour required by particles from the other two synthesis procedures. This water dispersibility was due to high amount of hydrophilic PAA absorbed on MMPs in one-step hydrothermal synthesis, which was also responsible for the reduced aggregation among MMPs. The excellent water dispersibility of PAA-MMPs prepared from this synthesis method extended to even after one-month storage.

PAA-MNPs formed via two-step hydrothermal synthesis procedure exhibited different collected percentage for the three time intervals (Figure 3.9 (b)), indicating the low controllability of this synthesis procedure. Figure 3.9 (c) shows that PAA-coated MNPs formed by room-temperature coating bare MNPs were the hardest to be collected, as the average percentage of collected MNPs within 10 min was the lowest (~60%) among three synthesis procedures. The long sonication time of these MNPs experienced during the synthesis process may contribute to the breakage of large aggregates into small nanocrystals, and hence result in their slow mobility in water even under a magnetic field. Varying collected percentage of particles from the latter two synthesis procedures within different time intervals could also indirectly demonstrated their wide range of particle size. PAA-MNPs from the latter two synthesis procedures also experienced impeded water-dispersibility after one-month storage, probably due to the insufficient PAA coating. Although collected particles from the latter two synthesis procedures took a relatively longer time, the collected percentage was near 100% after 24h, indicating a decent recyclability.

The difference of these particles' magnetic collection efficiency implied their different potential applications. PAA-MMPs from one-step hydrothermal procedure

with high magnetic collection efficiency, fast mobility, and best magnetic response could be used for applications that are time sensitive and require quick separation, such as rapid capture and detection for pathogens. They are useful for applications that require comprehensive elimination of particles when completed, such as pollutant removal. Other PAA-MNPs could be applied in situations where time is less sensitive, but recyclability of the particles is necessary, such as the separation of non-threatening bacteria and food ingredients.

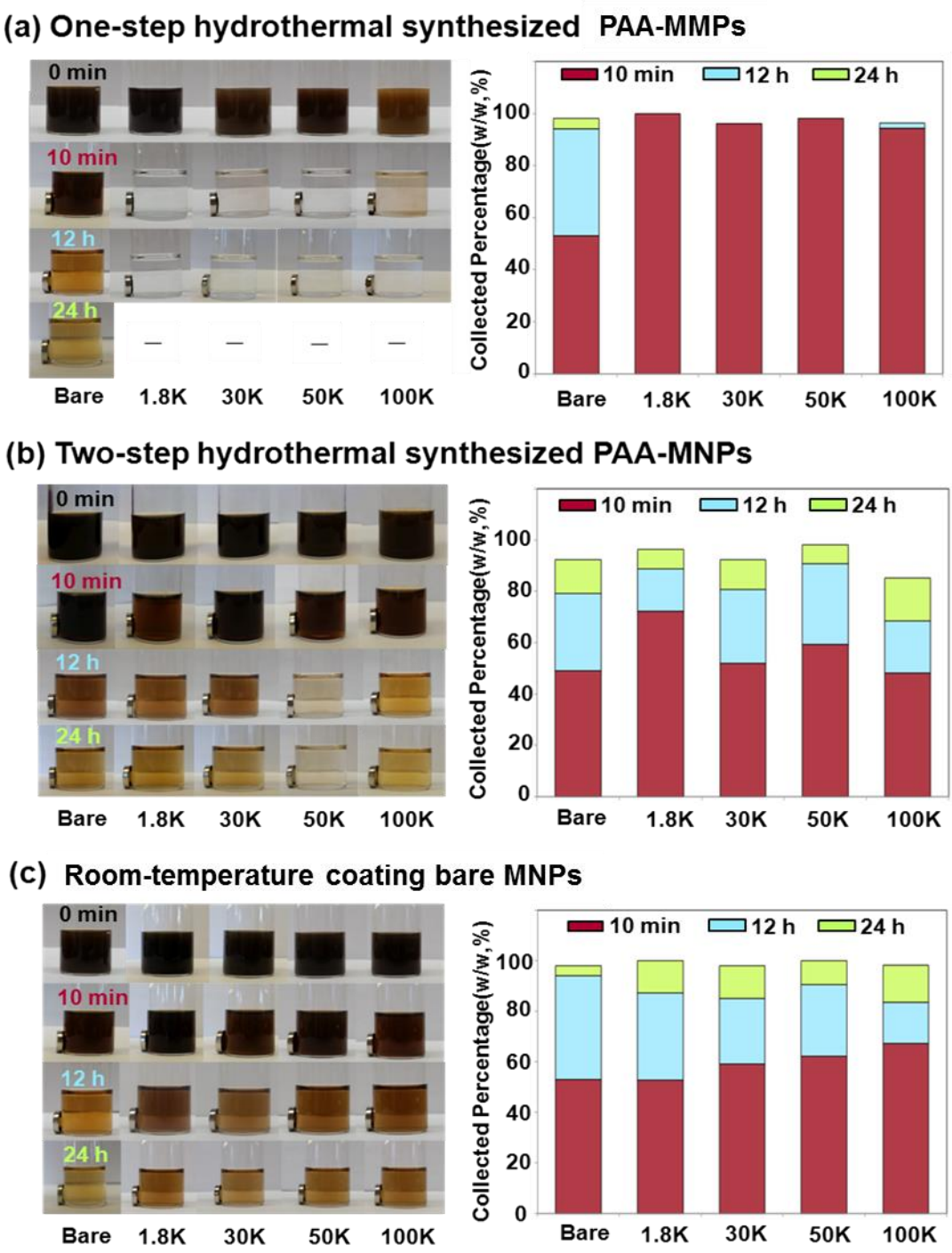

Figure 3.9 (a) - (c): Left: PAA-MMPs or PAA-MNPs suspension when a small magnet has been applied on the side wall after 0 min, 10 min, 12 h, and 24 h, respectively; Right: Percentage of the collected PAA-MMPs or PAA-MNPs

compared to the initial suspended amount after 10 min, 12 h, and 24 h of magnet application, respectively.

3.4 Potential Applications of PAA-coated Magnetic Particles

To explore the potential applications of PAA-MMPs, three experiments were conducted. In all experiments, the PAA-MMPs synthesized via one-step hydrothermal procedure were used, because they achieved the fastest magnetic collection from water and complete separation in a very short time.

3.4.1 Immobilization of Food Proteins and Enzymes

To evaluate the capability of the synthesized particles to conjugate proteins and enzymes, BSA and lysozyme (both at the concentration of 3 mg/ml) were selected for the experiments, and the conjugation degree was compared (Figure 3.10). The use of cross-linker EDC in pH 4.7 was to maximize the conjugation degree by covalently crosslinking the amino groups on proteins to the carboxyl groups on PAA-MMPs [70, 71]. The bare MNPs were also used to perform this conjugation study, as a control. It was expected that as PAA Mw increased and the particle size decreased, the conjugation degree would increase due to higher surface-to-volume ratio. It was also expected that bare MNPs would conjugate less amount of proteins, due to the lack of carboxyl groups from PAA. However, the results were not as expected, with the highest conjugation degree achieved by bare MNPs for both lysozyme (275 μg lysozyme per mg Fe_3O_4) and BSA (132 μg lysozyme per mg Fe_3O_4). This indicated the strong adsorption behavior of proteins on solid surfaces (such as Fe_3O_4 MPs) through mainly electrostatic and hydrophobic forces, which was also reported

elsewhere [70, 72, 73]. The PAA on the particle could decrease the adsorption by imposing steric hindrance against the adsorption of proteins onto Fe_3O_4 surfaces [74]. The Mw of polymer and the surface grafting density of polymer on a solid surface greatly affect the amount of adsorbed proteins [74]. The higher Mw and grafting density of polymer result in a thicker polymer layer, which will decrease the protein adsorption. In the current study, the conjugation degree of PAA-100K MMPs with BSA was the lowest, which may be attributed to the strong blocking effect of PAA layer. It was also evidenced by TG analysis that PAA-100K MMPs contained the highest amount of PAA per unit mass of Fe_3O_4 magnetic cores. PAA-1.8K MMPs achieved the second least conjugation degree, which may be also attributed to the relatively high amount of PAA on particles. The non-uniformed and aggregated morphology of PAA-1.8K MMPs may further reduce the available surface and block the incoming protein molecules as well. This blocking effect allows applications of PAA-MMPs as protein-resistant ("non-fouling") surfaces.

Moreover, for all MMPs that contained PAA, the conjugation degree for lysozyme was much higher than BSA at the same initial protein concentration. The highest conjugation degree of lysozyme was achieved by PAA-50K MMPs (147 μg lysozyme per mg Fe_3O_4 magnetic cores). And it was 88 μg BSA per mg Fe_3O_4 magnetic cores when BSA was conjugated with PAA-30K MMPs.

This huge difference could be explained by two reasons. On one hand, the smaller size of lysozyme (D_H ~4 nm [75]) compared to BSA (D_H ~7 nm [76]) permitted more lysozyme molecules to covalently conjugated on the surface of an individual PAA-MMP. The relatively smaller size of lysozyme also allowed itself to diffuse

through the PAA layer more easily and hence absorb on the Fe_3O_4 surface. On the other hand, the conjugation degree is also influenced by the electrostatic charge of PAA-MMPs and proteins [74]. The pH in the studied system was 7.0, which was below the isoelectric point (pI) of lysozyme (~ 11.35) but higher than the pKa of PAA (~ 4.30) [77]. Therefore, lysozyme molecules were positively charged, while PAA molecules were negatively charged. The electrostatic attraction may consequently favor the conjugation between lysozymes and PAA-MMPs. By contrast, the pI of BSA was around 4.9, conferring negative surface charges to BSA molecules. Therefore, the electrostatic repulsion between BSA molecules and PAA-MMPs would lead to a declined conjugation degree.

This conjugation study implied the potential use of these PAA-MMPs in the immobilization of any positively charged or negatively charged enzymes, so as to stabilize and protect the enzymes against harsh processing conditions. Enzyme immobilization can also serve to improve the recyclability and reduce the loss of the conjugated enzymes.

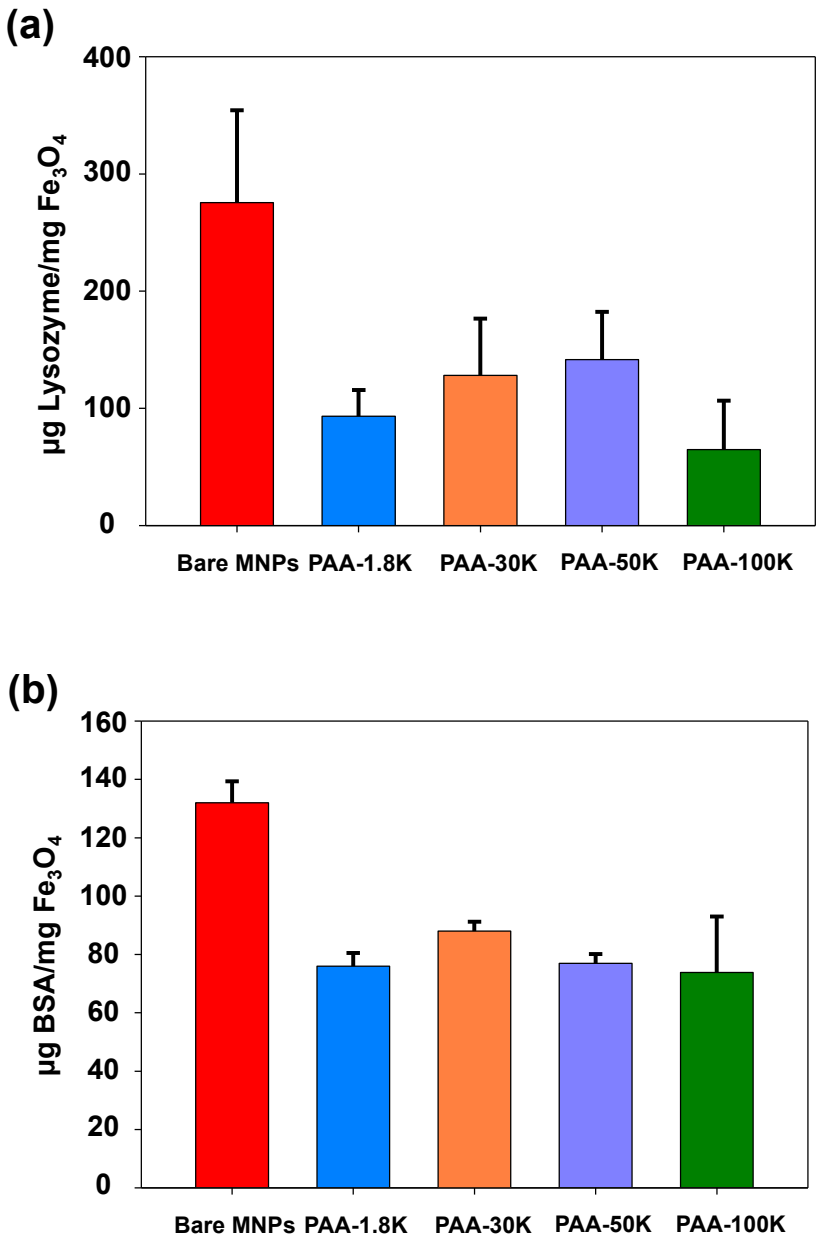

Figure 3.10 Conjugation degree of one-step hydrothermal synthesized PAA-MMPs with (a) 3mg/ml lysozyme (b) 3mg/ml BSA

3.4.2 Conjugation with Antibody and Capture of Food Pathogens

Antibodies are proteins that could specifically recognize a type of antigens. The fast capture and analysis of foodborne pathogens is significant to both food industries and customers. In this study, PAA-30K MMPs were selected to conjugate anti-*E. coli* IgG, which could recognize and capture the wild type *E. coli*. This *E. coli* has been engineered so that it could automatically emit red fluorescence. As demonstrated in Figure 3.11, large PAA-30K MMPs aggregates were found after the conjugation process. Figure 3.11 (a) are the images of PAA-30K MMPs without conjugated antibodies. Figure 3.11 (b) are the images of PAA-30K MMPs with antibodies conjugated on particles. Red fluorescence was observed in Figure 3.11 (b) but not in (a), implying the successful capture of *E. coli* by the anti-*E. coli* conjugated on PAA-30K MMPs. This study indicated the feasibility of rapid capture, separation, and concentration of foodborne pathogens by simply manipulating the MPs with an external magnetic field, as long as their antibodies are available.

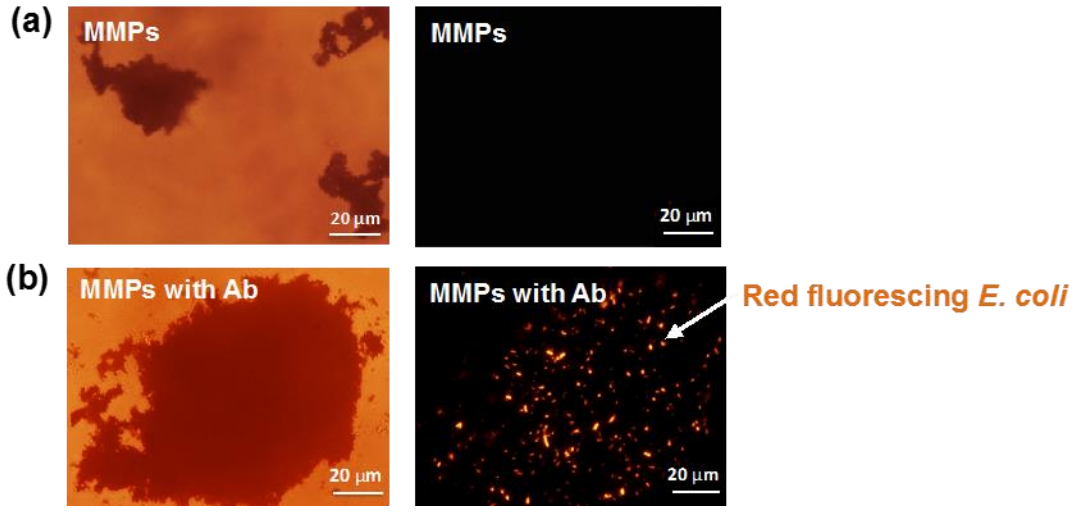

Figure 3.11 *E. coli* cells captured by (a) PAA-30K MMPs and (b) anti-*E. coli* conjugated PAA-30K MMPs, observed under bright field (left) and RFP channel (right) of a fluorescence microscopy.

(Exposure time = 100 ms, and magnefication = 40X)

3.4.3 Fabrication of Magnetic Hydrogel Films

Previous literature has revealed the feasibility of capturing and detecting foodborne pathogens using redox active magnetic hydrogel films [78, 79]. The fabrication of these magnetic hydrogel films was achieved through electrodeposition of MMPs-suspended chitosan solutions using a three-electrode system. Chitosan, a natural biopolymer rich in amino groups, was electrodeposited with a certain amount of suspended MMPs. During the electrodeposition, the chitosan molecules near the cathode electrode were initially dissolved in an acid solution, and became insoluble as the pH became basic when potential was applied to the electrode. The embedded MMPs in these deposited hydrogel films conferred them with magnetic property so that these films were able to magnetically attract free-floating MMPs with bound pathogen cells. Figure 3.12 shows the scheme of electrodeposition of chitosan with suspended MMPs [78].

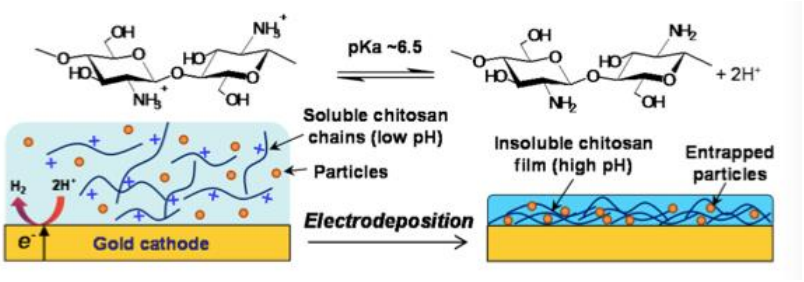

Figure 3.12 Scheme of electrodeposition of chitosan with suspended MMPs

In order to confer these electrodeposited magnetic hydrogel films with redox activity, they can be electrochemically modified by catechol molecules. This modification process is to oxidize catechol molecules into *o*-quinones, which subsequently graft onto amine-rich chitosan molecules. The catechol-grafted chitosan film serves as a redox capacitor to transfer electrons between oxidized and reduced forms of mediators and thus assist the redox-cycling near the surface of the gold electrode [80]. Without grafting catechol molecules, the redox-cycling is highly limited by the diffusion rate of the unconsumed mediators from the bulk solution to the gold electrode surface, since electrons transfer only occur within a very short distance from the gold electrode. After catechol molecules are grafted on the chitosan film, they rapidly accept and donate electrons from or to mediators; therefore to re-generate high concentrations of unconsumed mediators near the gold electrode surface, leading to amplification of output currents of the mediators (Figure 3.13) [80]. In the current study, Fc and PYO were selected as the mediators, which rapidly discharge and re-charge the non-conducting chitosan film in respect when the applied potential reaches to a certain value [80]. PYO was adopted as one of the redox mediators because it is a redox-active metabolite produced by *Pseudomonas*, which will be one of the targeted foodborne pathogens [80]. If *Pseudomonas* cells are present in a food sample, cyclic voltammograms (CV) could be further conducted to detect the concentration of the secreted PYO so as to determine the amount of *Pseudomonas* cells. Figure 3.14 demonstrated the cyclic voltammograms of output current before and after catechol modification of the chitosan films.

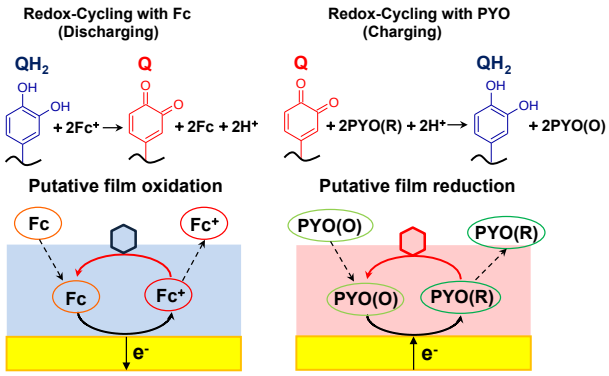

Figure 3.13 Typical redox-cycling among a catechol-grafted chitosan-MMPs film, a gold electrode, and mediators (Fc and PYO).

[Adapted from Ref 80 with permission of The Royal Society of Chemistry]

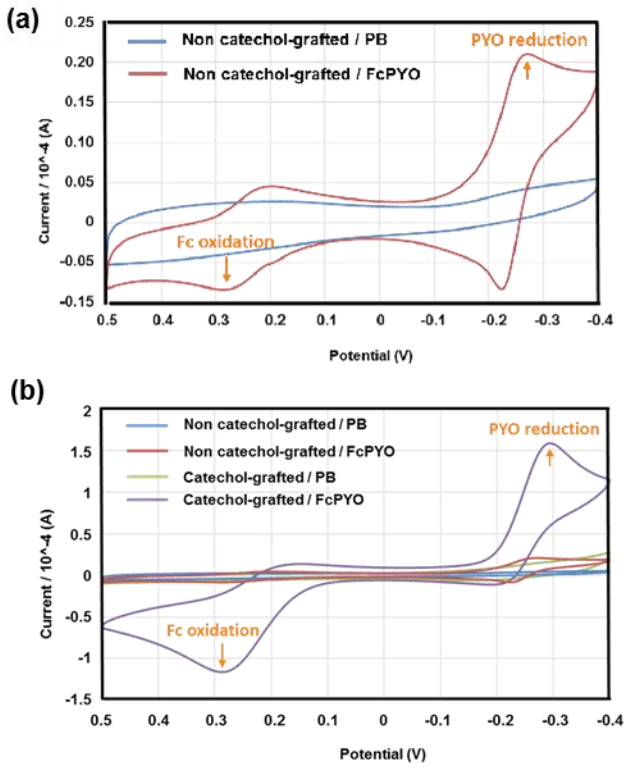

Figure 3.14 Cyclic voltammograms for (a) non catechol-grafted chitosan-MMPs film incubated with Fc and PYO; (b) catechol-grafted chitosan-MMPs film incubated with Fc and PYO.

It is worth mentioning that preliminary studies showed that direct one-step electro-deposition of chitosan-MMPs resulted in inhibited PYO reduction output current signal. This might be due to the steric hindrance imposed by the high concentration of MMPs near the gold electrode surface, which decelerated the diffusion of Fc and PYO, and decreased the effective electrode surface, both affecting the electrons transfer on the electrode. Therefore, all of the chitosan-MMPs films in this current study were fabricated by two-step electrodeposition, with the chitosan being the first layer of the film near the electrode, and chitosan-MMPs being the second layer.

This electrochemical study using Fc and PYO as electrons transfer mediators demonstrated that magnetic hydrogel catechol-grafted films could be used for foodborne pathogen detection in food safety analysis. Besides the potential application in pathogen detection, these films could also be utilized to acquire the global redox information from a biological system through a similar electrochemical approach.

CV of these chitosan-MMPs films with only the oxidizing mediator (Fc) was also performed after the first and second ascorbic acid treatment of the films (Figure 3.15). Compared to the aforementioned electrochemical re-charging by PYO, the catechol-grafted chitosan-MMPs films in this case were re-charged chemically using ascorbic acid as the reducing agent. When there was only Fc without PYO, the film was constantly discharged, hence only showing the oxidation peak for Fc, which declined as CV cycles continued [80]. After treating the films with ascorbic acid, it exhibited the same re-dox capability as that of the original. This suggested the

capability of these films to repeatedly obtain the redox information from a biological context, which may or may not contain redox-active substances such as ascorbic acid.

In brief, catechol-grafted chitosan-MMPs films were expected to establish a simple prototype for hydrogel films that possess both redox activity and magnetic property. The two-step electrodeposited film incorporated higher amount of MMPs while the redox signal remained uncompromised. With further investigation, these magnetic hydrogel films could be utilized to rapidly detect pathogens from a food matrix as well as to acquire the overall redox information demonstrated by a biological system through electrochemical approaches.

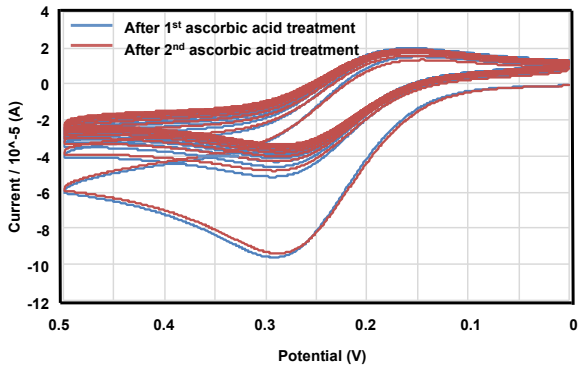

Figure 3.15 Cyclic voltammograms for a catechol-grafted chitosan-MMPs film incubated with only Fc mediator.

Chapter 4: Summary and Perspectives

4.1 Summary

PAA-coated MPs synthesized via three different hydrothermal procedures were characterized, and the effect of PAA Mw, synthesis temperature, and aging time on their size and morphology was studied. This study showed the controllability of particle size of MPs by adjusting these parameters. Through appropriate control, a series of MPs with different size could be synthesized, based on the demand of different applications. Furthermore, it was found that super-paramagnetic Fe_3O_4 MPs with pronounced water-dispersibility, minor aggregation, and exceptional magnetic response could be efficiently synthesized via one-step hydrothermal procedure using only simple ingredients like high Mw PAA. This simple synthesis avoided tedious synthesis steps while yielding MPs with remarkable features suitable for versatile applications. Three potential applications involving PAA-MMPs formed by one-step hydrothermal procedure were explored. The successful immobilization of BSA and lysozyme expected the wide-range uses of PAA-MMPs in food industry. The successful capture of *E. coli* using MMPs-antibody conjugates indicated the feasibility of rapid immunomagnetic capture and separation of pathogens or toxins in food safety analyses. PAA-MMPs could also be involved in the fabrication of magnetic hydrogel films, which could capture pathogens or toxins bound MMPs or and quantify those pathogens or toxins via electrochemical approaches.

4.2 Future Studies

While the synthesized PAA-MMPs possess appealing characteristics and are convenient to use, further studies are needed to overcome several weakness or confer them with innovative features. Firstly, although PAA is a non-toxic polymer, it is synthetic and not classified as biodegradable. The use of PAA-MMPs in food industry may trigger safety concerns, except for applications that avoid food ingredients, such as pathogen immune-separation in food safety analysis and water treatment in environmental management. The feasibility of synthesizing MPs with similar properties but using alternative food polymers with high Mw could be researched. Secondly, more studies pertaining to the pathogen capture and electrochemical detection could be conducted. The condition to immobilize the highest amount of antibodies and *E. coli* cells on PAA-MMPs could be researched, and the magnetic properties as well as the redox activities of the magnetic hydrogel films could also be optimized. Thirdly, PAA-MNPs synthesized from the latter two hydrothermal synthesis procedures were relatively more prone to aggregation probably due to the lack of sufficient polymer layer. Therefore, the amount of polymer required in synthesis to obtain appealing particles could be further researched. Lastly, more functional groups could be engineered on the current carboxyl-containing magnetic particles, accommodating diverse applications.

References

1. Issa, B.; Obaidat, I. M.; Albiss, B. A.; Haik, Y., Magnetic nanoparticles: surface effects and properties related to biomedicine applications. *International journal of molecular sciences* **2013**, *14*, 21266-21305.
2. Caruntu, D.; Caruntu, G.; O'Connor, C. J., Magnetic properties of variable-sized Fe3O4 nanoparticles synthesized from non-aqueous homogeneous solutions of polyols. *Journal of physics D: Applied physics* **2007**, *40*, 5801.
3. Awschalom, D. D.; DiVincenzo, D. P., Complex dynamics of mescoscopic magnets. *Physics Today* **1995**, *48*, 43-48.
4. Kodama, R.; Berkowitz, A.; McNiff Jr, E.; Foner, S., Surface spin disorder in ferrite nanoparticles. *Journal of Applied Physics* **1997**, *81*, 5552-5557.
5. Morales, M. d. P.; Veintemillas-Verdaguer, S.; Montero, M.; Serna, C.; Roig, A.; Casas, L.; Martinez, B.; Sandiumenge, F., Surface and internal spin canting in γ -Fe2O3 nanoparticles. *Chemistry of Materials* **1999**, *11*, 3058-3064.
6. Si, S.; Kotal, A.; Mandal, T. K.; Giri, S.; Nakamura, H.; Kohara, T., Size-controlled synthesis of magnetite nanoparticles in the presence of polyelectrolytes. *Chemistry of Materials* **2004**, *16*, 3489-3496.
7. Singamaneni, S.; Bliznyuk, V. N.; Binek, C.; Tsymbal, E. Y., Magnetic nanoparticles: recent advances in synthesis, self-assembly and applications. *Journal of Materials Chemistry* **2011**, *21*, 16819-16845.
8. Wu, W.; He, Q.; Jiang, C., Magnetic iron oxide nanoparticles: synthesis and surface functionalization strategies. *ChemInform* **2009**, *40*, i.
9. Lopez Perez, J.; Lopez Quintela, M.; Mira, J.; Rivas, J.; Charles, S., Advances in the preparation of magnetic nanoparticles by the microemulsion method. *The Journal of Physical Chemistry B* **1997**, *101*, 8045-8047.
10. Santra, S.; Tapec, R.; Theodoropoulou, N.; Dobson, J.; Hebard, A.; Tan, W., Synthesis and characterization of silica-coated iron oxide nanoparticles in microemulsion: the effect of nonionic surfactants. *Langmuir* **2001**, *17*, 2900-2906.
11. Vuong, T. K. O.; Le, T. L.; Pham, D. V.; Pham, H. N.; Le Ngo, T. H.; Do, H. M.; Nguyen, X. P., Synthesis of high-magnetization and monodisperse Fe 3 O 4 nanoparticles via thermal decomposition. *Materials Chemistry and Physics* **2015**, *163*, 537-544.
12. Amara, D.; Felner, I.; Nowik, I.; Margel, S., Synthesis and characterization of Fe and Fe 3 O 4 nanoparticles by thermal decomposition of triiron dodecacarbonyl. *Colloids and Surfaces A: Physicochemical and Engineering Aspects* **2009**, *339*, 106-110.
13. Su, G.; Lu, H.; Zhang, L.; Zhang, A.; Huang, L.; Liu, S.; Li, L.; Zheng, M., Thermal degradation of octachloronaphthalene over as-prepared Fe3O4 micro/nanomaterial and its hypothesized mechanism. *Environmental science & technology* **2014**, *48*, 6899-6908.
14. Park, J.; Lee, E.; Hwang, N.-M.; Kang, M.; Kim, S. C.; Hwang, Y.; Park, J.-G.; Noh, H.-J.; Kim, J.-Y.; Park, J.-H.; Hyeon, T., One-Nanometer-Scale Size-Controlled Synthesis of Monodisperse Magnetic Iron Oxide Nanoparticles. *Angewandte Chemie International Edition* **2005**, *44*, 2872-2877.
15. Sun, S.; Zeng, H., Size-controlled synthesis of magnetite nanoparticles. *Journal of the American Chemical Society* **2002**, *124*, 8204-8205.

16. Qian, Y.; Xie, Y.; He, C.; Li, J.; Chen, Z., Hydrothermal preparation and characterization of ultrafine magnetite powders. *Materials research bulletin* **1994**, *29*, 953-957.
17. Tao, K.; Song, S.; Ding, J.; Dou, H.; Sun, K., Carbonyl groups anchoring for the water dispersibility of magnetite nanoparticles. *Colloid and Polymer Science* **2011**, *289*, 361-369.
18. Eberbeck, D.; Kettering, M.; Bergemann, C.; Zirpel, P.; Hilger, I.; Trahms, L., Quantification of the aggregation of magnetic nanoparticles with different polymeric coatings in cell culture medium. *Journal of Physics D: Applied Physics* **2010**, *43*, 405002.
19. Huang, Y.-F.; Wang, Y.-F.; Yan, X.-P., Amine-functionalized magnetic nanoparticles for rapid capture and removal of bacterial pathogens. *Environmental science & technology* **2010**, *44*, 7908-7913.
20. Sun, Y.; Ding, X.; Zheng, Z.; Cheng, X.; Hu, X.; Peng, Y., A novel approach to magnetic nanoadsorbents with high binding capacity for bovine serum albumin. *Macromolecular rapid communications* **2007**, *28*, 346-351.
21. Zhang, S.; Zhang, Y.; Liu, J.; Xu, Q.; Xiao, H.; Wang, X.; Xu, H.; Zhou, J., Thiol modified Fe 3 O 4@ SiO 2 as a robust, high effective, and recycling magnetic sorbent for mercury removal. *Chemical engineering journal* **2013**, *226*, 30-38.
22. He, Y.; Wang, S.; Li, C.; Miao, Y.; Wu, Z.; Zou, B., Synthesis and characterization of functionalized silica-coated Fe3O4 superparamagnetic nanocrystals for biological applications. *Journal of Physics D: Applied Physics* **2005**, *38*, 1342.
23. Gref, R.; Domb, A.; Quellec, P.; Blunk, T.; Müller, R.; Verbavatz, J.; Langer, R., The controlled intravenous delivery of drugs using PEG-coated sterically stabilized nanospheres. *Advanced drug delivery reviews* **2012**, *64*, 316-326.
24. Yu, M.; Huang, S.; Yu, K. J.; Clyne, A. M., Dextran and polymer polyethylene glycol (PEG) coating reduce both 5 and 30 nm iron oxide nanoparticle cytotoxicity in 2D and 3D cell culture. *International journal of molecular sciences* **2012**, *13*, 5554-5570.
25. Mikhaylova, M.; Kim, D. K.; Berry, C. C.; Zagorodni, A.; Toprak, M.; Curtis, A. S.; Muhammed, M., BSA immobilization on amine-functionalized superparamagnetic iron oxide nanoparticles. *Chemistry of materials* **2004**, *16*, 2344-2354.
26. Lewin, M.; Carlesso, N.; Tung, C.-H.; Tang, X.-W.; Cory, D.; Scadden, D. T.; Weissleder, R., Tat peptide-derivatized magnetic nanoparticles allow in vivo tracking and recovery of progenitor cells. *Nature biotechnology* **2000**, *18*, 410-414.
27. Shete, P.; Patil, R.; Tiwale, B.; Pawar, S., Water dispersible oleic acid-coated Fe 3 O 4 nanoparticles for biomedical applications. *Journal of Magnetism and Magnetic Materials* **2015**, *377*, 406-410.
28. Gupta, A. K.; Gupta, M., Synthesis and surface engineering of iron oxide nanoparticles for biomedical applications. *Biomaterials* **2005**, *26*, 3995-4021.
29. Sahoo, Y.; Goodarzi, A.; Swihart, M. T.; Ohulchanskyy, T. Y.; Kaur, N.; Furlani, E. P.; Prasad, P. N., Aqueous ferrofluid of magnetite nanoparticles: fluorescence labeling and magnetophoretic control. *The Journal of Physical Chemistry B* **2005**, *109*, 3879-3885.
30. Sousa, M.; Rubim, J.; Sobrinho, P.; Tourinho, F., Biocompatible magnetic fluid precursors based on aspartic and glutamic acid modified maghemite nanostructures. *Journal of magnetism and magnetic materials* **2001**, *225*, 67-72.
31. Li, G.-y.; Huang, K.-l.; Jiang, Y.-r.; Ding, P.; Yang, D.-l., Preparation and characterization of carboxyl functionalization of chitosan derivative magnetic nanoparticles. *Biochemical Engineering Journal* **2008**, *40*, 408-414.
32. Liao, M.-H.; Chen, D.-H., Preparation and characterization of a novel magnetic nano-adsorbent. *Journal of Materials Chemistry* **2002**, *12*, 3654-3659.

33. Yang, X.; Jiang, W.; Liu, L.; Chen, B.; Wu, S.; Sun, D.; Li, F., One-step hydrothermal synthesis of highly water-soluble secondary structural Fe 3 O 4 nanoparticles. *Journal of Magnetism and Magnetic Materials* **2012**, *324*, 2249-2257.
34. Wu, W.; He, Q.; Chen, H.; Tang, J.; Nie, L., Sonochemical synthesis, structure and magnetic properties of air-stable Fe3O4/Au nanoparticles. *Nanotechnology* **2007**, *18*, 145609.
35. Al-Sayari, S.; Carley, A. F.; Taylor, S. H.; Hutchings, G. J., Au/ZnO and Au/Fe2O3 catalysts for CO oxidation at ambient temperature: comments on the effect of synthesis conditions on the preparation of high activity catalysts prepared by coprecipitation. *Topics in Catalysis* **2007**, *44*, 123-128.
36. Wang, D.; He, J.; Rosenzweig, N.; Rosenzweig, Z., Superparamagnetic Fe2O3 beads-CdSe/ZnS quantum dots core-shell nanocomposite particles for cell separation. *Nano Letters* **2004**, *4*, 409-413.
37. Manent, J.; Oguievetskaia, K.; Bayer, J.; Ratner, N.; Giovannini, M., Magnetic cell sorting for enriching Schwann cells from adult mouse peripheral nerves. *Journal of neuroscience methods* **2003**, *123*, 167-173.
38. Jain, T. K.; Morales, M. A.; Sahoo, S. K.; Leslie-Pelecky, D. L.; Labhasetwar, V., Iron oxide nanoparticles for sustained delivery of anticancer agents. *Molecular pharmaceutics* **2005**, *2*, 194-205.
39. Khoshnevisan, K.; Bordbar, A.-K.; Zare, D.; Davoodi, D.; Noruzi, M.; Barkhi, M.; Tabatabaei, M., Immobilization of cellulase enzyme on superparamagnetic nanoparticles and determination of its activity and stability. *Chemical engineering journal* **2011**, *171*, 669-673.
40. Namdeo, M.; Bajpai, S., Immobilization of α -amylase onto cellulose-coated magnetite (CCM) nanoparticles and preliminary starch degradation study. *Journal of Molecular Catalysis B: Enzymatic* **2009**, *59*, 134-139.
41. Sun, J.; Su, Y.; Rao, S.; Yang, Y., Separation of lysozyme using superparamagnetic carboxymethyl chitosan nanoparticles. *Journal of Chromatography B* **2011**, *879*, 2194-2200.
42. Zhang, G.; Cao, Q.; Li, N.; Li, K.; Liu, F., Tris (hydroxymethyl) aminomethane-modified magnetic microspheres for rapid affinity purification of lysozyme. *Talanta* **2011**, *83*, 1515-1520.
43. Cao, M.; Li, Z.; Wang, J.; Ge, W.; Yue, T.; Li, R.; Colvin, V. L.; William, W. Y., Food related applications of magnetic iron oxide nanoparticles: enzyme immobilization, protein purification, and food analysis. *Trends in Food Science & Technology* **2012**, *27*, 47-56.
44. Wang, H.; Huang, J.; Wang, C.; Li, D.; Ding, L.; Han, Y., Immobilization of glucose oxidase using CoFe 2 O 4/SiO 2 nanoparticles as carrier. *Applied Surface Science* **2011**, *257*, 5739-5745.
45. Wu, X.; Hu, J.; Zhu, B.; Lu, L.; Huang, X.; Pang, D., Aptamer-targeted magnetic nanospheres as a solid-phase extraction sorbent for determination of ochratoxin A in food samples. *Journal of Chromatography A* **2011**, *1218*, 7341-7346.
46. Arora, P.; Sindhu, A.; Dilbaghi, N.; Chaudhury, A., Biosensors as innovative tools for the detection of food borne pathogens. *Biosensors and Bioelectronics* **2011**, *28*, 1-12.
47. Varshney, M.; Li, Y., Interdigitated array microelectrode based impedance biosensor coupled with magnetic nanoparticle–antibody conjugates for detection of Escherichia coli O157: H7 in food samples. *Biosensors and Bioelectronics* **2007**, *22*, 2408-2414.
48. Varshney, M.; Yang, L.; Su, X.-L.; Li, Y., Magnetic nanoparticle-antibody conjugates for the separation of Escherichia coli O157: H7 in ground beef. *Journal of Food Protection®* **2005**, *68*, 1804-1811.

49. Kim, E.; Gordonov, T.; Bentley, W. E.; Payne, G. F., Amplified and in situ detection of redox-active metabolite using a biobased redox capacitor. *Analytical chemistry* **2013**, *85*, 2102-2108.
50. Chaki, S.; Malek, T. J.; Chaudhary, M.; Tailor, J.; Deshpande, M., Magnetite Fe3O4 nanoparticles synthesis by wet chemical reduction and their characterization. *Advances in Natural Sciences: Nanoscience and Nanotechnology* **2015**, *6*, 035009.
51. Monshi, A.; Foroughi, M. R.; Monshi, M. R., Modified Scherrer equation to estimate more accurately nano-crystallite size using XRD. *World Journal of Nano Science and Engineering* **2012**, *2*, 154.
52. Tomaszewski, P. E., The uncertainty in the grain size calculation from X-ray diffraction data. *Phase Transitions* **2013**, *86*, 260-266.
53. Nassima, O.; Samir, F.; Silvana, M.; Fatih, Z.; Frédéric, S.; Noureddine, J.; Ivaylo, H.; Guillaume, W.; Christian, R., Magnetic nanowire synthesis: A chemical engineering approach. *AIChE Journal* **2015**, *61*, 304-316.
54. Thakur, V. K.; Thakur, M. K., *Eco-friendly Polymer Nanocomposites: Chemistry and Applications*. Springer: 2015; Vol. 74.
55. Zheng, Y.-h.; Cheng, Y.; Bao, F.; Wang, Y.-s., Synthesis and magnetic properties of Fe 3 O 4 nanoparticles. *Materials research bulletin* **2006**, *41*, 525-529.
56. Xuan, S.; Wang, Y.-X. J.; Yu, J. C.; Cham-Fai Leung, K., Tuning the grain size and particle size of superparamagnetic Fe3O4 microparticles. *Chemistry of Materials* **2009**, *21*, 5079-5087.
57. Moeser, G. D.; Green, W. H.; Laibinis, P. E.; Linse, P.; Hatton, T. A., Structure of polymer-stabilized magnetic fluids: Small-angle neutron scattering and mean-field lattice modeling. *Langmuir* **2004**, *20*, 5223-5234.
58. Kislenko, V., Polymer Adsorption at Solid Surfaces: Theoretical Aspects. *ChemInform* **2013**, *44*.
59. Eggert, A. R., The role of particle size and molecular weight on the adsorption and flocculation of polystyrene latex with poly (1, 2-dimethyl-5-vinylpyridinium bromide). **1976**.
60. Das, K. K.; Somasundaran, P., A kinetic investigation of the flocculation of alumina with polyacrylic acid. *Journal of colloid and interface science* **2004**, *271*, 102-109.
61. Xu, C.; Teja, A. S., Continuous hydrothermal synthesis of iron oxide and PVA-protected iron oxide nanoparticles. *The Journal of Supercritical Fluids* **2008**, *44*, 85-91.
62. Alfaro, S.; Rodriguez, C.; Valenzuela, M.; Bosch, P., Aging time effect on the synthesis of small crystal LTA zeolites in the absence of organic template. *Materials Letters* **2007**, *61*, 4655-4658.
63. Gubicza, J.; Labar, J. L.; Quynh, L. M.; Nam, N. H.; Luong, N. H., Evolution of size and shape of gold nanoparticles during long-time aging. *Materials Chemistry and Physics* **2013**, *138*, 449-453.
64. Sun, X.; Sun, K.; Liang, Y., Hydrothermal synthesis of magnetite: investigation of influence of aging time and mechanism. *Micro & Nano Letters, IET* **2015**, *10*, 99-104.
65. Reith, D.; Müller, B.; Müller-Plathe, F.; Wiegand, S., How does the chain extension of poly (acrylic acid) scale in aqueous solution? A combined study with light scattering and computer simulation. *The Journal of chemical physics* **2002**, *116*, 9100-9106.
66. Kodama, R., Magnetic nanoparticles. *Journal of Magnetism and Magnetic Materials* **1999**, *200*, 359-372.
67. Levy, M.; Quarta, A.; Espinosa, A.; Figuerola, A.; Wilhelm, C.; García-Hernández, M.; Genovese, A.; Falqui, A.; Alloyeau, D.; Buonsanti, R., Correlating magneto-structural

properties to hyperthermia performance of highly monodisperse iron oxide nanoparticles prepared by a seeded-growth route. *Chemistry of Materials* **2011**, *23*, 4170-4180.
68. Sun, X.; Sun, K.; Wang, S.; Zhang, S.; Liu, Z.; Wang, Y., Preparation of hydrophobic magnetite by a simple solvothermal method using oleylamine as reducing and surface modification agent. *IET Micro & Nano Letters* **2016**, *11*, 118-121.
69. Das, H.; Sakamoto, N.; Aono, H.; Shinozaki, K.; Suzuki, H.; Wakiya, N., Investigations of superparamagnetism in magnesium ferrite nano-sphere synthesized by ultrasonic spray pyrolysis technique for hyperthermia application. *Journal of Magnetism and Magnetic Materials* **2015**, *392*, 91-100.
70. Peng, Z.; Hidajat, K.; Uddin, M., Conformational change of adsorbed and desorbed bovine serum albumin on nano-sized magnetic particles. *Colloids and Surfaces B: Biointerfaces* **2004**, *33*, 15-21.
71. Vashist, S. K., Comparison of 1-ethyl-3-(3-dimethylaminopropyl) carbodiimide based strategies to crosslink antibodies on amine-functionalized platforms for immunodiagnostic applications. *Diagnostics* **2012**, *2*, 23-33.
72. Norde, W.; Anusiem, A. C., Adsorption, desorption and re-adsorption of proteins on solid surfaces. *Colloids and Surfaces* **1992**, *66*, 73-80.
73. Giacomelli, C. E.; Avena, M. J.; De Pauli, C. P., Adsorption of bovine serum albumin onto TiO 2 particles. *Journal of colloid and interface science* **1997**, *188*, 387-395.
74. Pasche, S.; Textor, M.; Meagher, L.; Spencer, N. D.; Griesser, H. J., Relationship between interfacial forces measured by colloid-probe atomic force microscopy and protein resistance of poly (ethylene glycol)-grafted poly (L-lysine) adlayers on niobia surfaces. *Langmuir* **2005**, *21*, 6508-6520.
75. Zhang, Y.; Farrell, E.; Mankiewicz, D.; Weiner, Z., Study of Protein Hydrodynamics with Light Scatter-ing: Size and Charge of Lysozyme.
76. Yohannes, G.; Wiedmer, S. K.; Elomaa, M.; Jussila, M.; Aseyev, V.; Riekkola, M.-L., Thermal aggregation of bovine serum albumin studied by asymmetrical flow field-flow fractionation. *Analytica chimica acta* **2010**, *675*, 191-198.
77. Zhang, S.; Shu, X.; Zhou, Y.; Huang, L.; Hua, D., Highly efficient removal of uranium (VI) from aqueous solutions using poly (acrylic acid)-functionalized microspheres. *Chemical Engineering Journal* **2014**, *253*, 55-62.
78. Li, Y.; Liu, Y.; Gao, T.; Zhang, B.; Song, Y.; Terrell, J. L.; Barber, N.; Bentley, W. E.; Takeuchi, I.; Payne, G. F., Self-Assembly with Orthogonal-Imposed Stimuli To Impart Structure and Confer Magnetic Function To Electrodeposited Hydrogels. *ACS applied materials & interfaces* **2015**, *7*, 10587-10598.
79. Kim, E.; Gordonov, T.; Liu, Y.; Bentley, W. E.; Payne, G. F., Reverse engineering to suggest biologically relevant redox activities of phenolic materials. *ACS chemical biology* **2013**, *8*, 716-724.
80. Kim, E.; Liu, Y.; Bentley, W. E.; Payne, G. F., Redox Capacitor to Establish Bio‐Device Redox‐Connectivity. *Advanced Functional Materials* **2012**, *22*, 1409-1416.